Ivo Aguiar Maceira

Evolução temporal de estados localizados da rede de Lieb

Time evolution of localized states of the Lieb lattice

Ivo Aguiar Maceira

Evolução temporal de estados localizados da rede de Lieb

Time evolution of localized states of the Lieb lattice

Dissertação apresentada à Universidade de Aveiro para cumprimento dos requesitos necessários à obtenção do grau de Mestre em Física, realizada sob a orientação científica de Ricardo Assis Guimarães Dias, professor do Departamento de Física da Universidade de Aveiro

o júri / the jury

presidente / president

Manuel António dos Santos Barroso
Professor Auxiliar da Universidade de Aveiro

vogais / examiners committee

Iveta Rombeiro do Rego Pimentel
Professora Associada da Universidade de Lisboa

Ricardo Assis Guimarães Dias
Professor Auxiliar da Universidade de Aveiro (orientador)

agradecimentos / acknowledgements

Agradeço ao Daniel Gouveia pela sua colaboração neste trabalho.

Resumo

Nesta tese, estudamos a evolução temporal de estados localizados da rede de Lieb quando aplicamos um campo magnético perpendicular à rede que aumenta em intensidade linearmente e lentamente. Começamos por estudar a evolução temporal analiticamente, usando propriedades de simetria do modelo de tight-binding da rede de Lieb. Esta análise revela a importância do campo eléctrico gerado pelo campo magnético variável no tempo para a evolução temporal. De seguida mostramos os resultados numéricos da evolução temporal de estados inicialmente localizados. Nas simulações encontramos um comportamento em forma de escada na componente localizada do estado em evolução que só se manifesta quando o campo eléctrico não é invariante por rotações à volta do centro da rede. Mostramos que a evolução de estados inicialmente localizados da rede de Lieb pode ser aproximada de forma muito precisa usando um sistema de três níveis que se torna num sistema de precessão clássico quando as entradas da matriz de evolução são todas reais.

Abstract

We study the time evolution of localized states of the Lieb lattice when a magnetic flux is applied perpendicularly to the lattice and increased slowly and linearly in time. The time evolution is first studied analytically, making use of several symmetry properties of the Lieb tight-binding model, showing the importance of the electric field generated by the time dependent magnetic field in the evolution. We present numerical simulation results of the time evolution of initially localized states, which feature a characteristic step pattern of the localized component when the electric field is not invariant under rotations around the center of the lattice. We show how the evolution of Lieb localized states can be approximated very effectively using a three level system that, for real matrix entries, is a classical precession system.

Contents

List of Figures

Chapter 1

Introduction

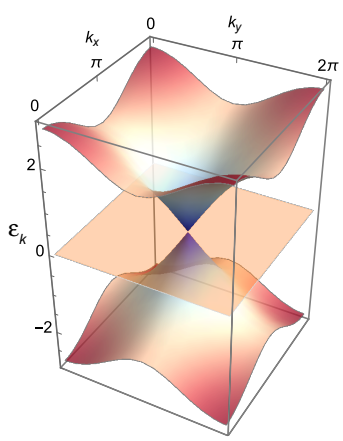

Figure 1.1: Energy bands of the Lieb lattice.

The Lieb (line centred square) lattice is a 2D decorated lattice that features three energy bands in its tight-binding model[1] (Fig. 1.1), one of them flat (zero dispersion). The flat band is a high degeneracy energy subspace composed of localized states. Other 2D lattices also have flat bands, like the kagomé (trihexagonal),[2] Mielke (chequerboard),[3] and Tasaki[4] lattices. There are methods of finding a localized state of a lattice knowing a localized state of a different lattice,[5] and also of constructing lattices with flat bands starting from chains with flat bands.[6] An example of a chain with flat band is the AB_2 chain.[7] Both the Lieb lattice and the AB_2 chain have their flat band in-between two itinerant bands. In all the other lattices mentioned, the flat band is a degenerate ground subspace. The flat band of the Lieb lattice and the AB_2 chain are retained when a magnetic field perpendicular to the lattice or chain is applied, meaning localized states still exist even under a magnetic field, which does not occur in the other mentioned lattices. The common property of the Lieb lattice and the AB_2 chain that distinguishes them from the rest is that they are bipartite lattices. The bipartite lattice property is necessary for the robustness of the flat-bands against external magnetic fields to occur, as discussed in section 2.5.

The search for flat-band ferromagnetism has been the main motivation in the theoretical research of flat-band systems for some time,[8,4,9,10] including the particular case of the Lieb lattice.[11,12] On the experimental side, azurite is a promising material in what concerns the observation of flat-band physics since it can be approximately described as an AB_2 chain.[13] The copper oxide planes of high temperature of cuprate superconductors such as $La_{2-x}Sr_xCuO_4$ and $YBa_2Cu_3O_7$ have a structure resembling the Lieb lattice.[14,15] The use of quantum dot arrays with the desired geometry is one of the proposed methods for building flat band systems.[16] Recent experimental realizations of flat-band systems include exciton-polariton condensates in a 2D kagomé lattice[17] and in

a 1D Lieb lattice.[18] Also, localized states were realized in a photonic Lieb lattice formed by an array of optical waveguides.[19,20] The destructive interference characteristic of localized states allows for diffractionless localized conduction of light over long distances. Systems of cold atoms trapped in optical Lieb lattices have been proposed as research tools to study both flat band ferromagnetism,[21,11] and the field of topological phases,[22] and recent success has been reported in the realization of such a system.[23]

Motivation

Contrary to other decorated lattices, the flat band of the Lieb lattice is retained when a magnetic field perpendicular to the lattice is applied, meaning localized states still exist even under a magnetic field. To further test the robustness of the Lieb localized states under magnetic fields, we enquired the following - does an electron in a localized state of the Lieb lattice continue to be localized if we slowly increase an applied, perpendicular, magnetic field? An answer can be achieved by numerical simulations of said system, which were carried out. The simulations revealed a step-like pattern of the localized component. This pattern incited further investigation and a three level toy model was conceived that exhibited an identical evolution pattern. After this, a general and rigorous analytical approach to the time evolution was deemed necessary and was developed. It revealed the importance for the time evolution of the system symmetries and of the electric field created by the time dependent magnetic field. The analytical results also helped to more naturally deduce the three level approximation.

Outline

We start with a review of the tight-binding model of the Lieb lattice in chapter 2, with an emphasis on the localized states and on the relevant symmetries. The time evolution on the Lieb lattice through analytical means is addressed in chapter 3, making use of the properties described in the previous chapter. In chapter 4, we present the simulation results and analysis, where we calculate the localized and itinerant components of an initially localized state over time as we slowly increase the magnetic field. In chapter 5 the three level model is introduced and we discuss its classical interpretation and how it is able to reproduce the step-like pattern found in the simulations.

Chapter 2

Lieb Lattice

In this chapter we start with a review of the tight-binding model of the Lieb lattice and the states that form the Lieb flat band, first without and after with an external magnetic field applied. We then analyse the $\pm E$ symmetry (or particle-hole symmetry), which is a consequence of the Lieb lattice being bipartite, and also the point group invariances of the eigenstates. We finish with the energy diagram as a function of the magnetic flux.

2.1 Tight-binding model

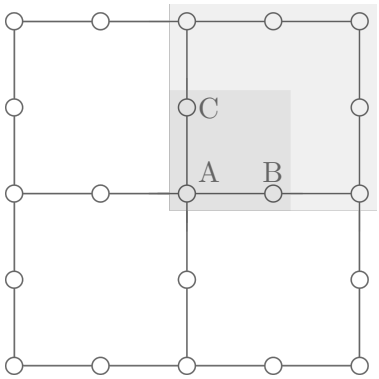

Figure 2.1: 2×2 Lieb lattice. In darker grey, a unit cell. In lighter grey, a plaquette.

The Lieb lattice is a decorated lattice that can be built by the introduction of an atom (or ion) between nearest neighbour atoms of a 2D square lattice (Fig. 2.1). This gives rise to a lattice with two types of atoms: one has four neighbours, which we will call a type A site, and the other has two, a type BC. We can distinguish further between atoms that have two horizontal neighbours, type B, and two vertical, type C. The unit cell consists of three atoms, an A, a B, and a C. We can also label the atoms by their Cartesian coordinates, which will be a more useful notation for some calculations. The size of the lattice is given by the number of unit cells in each dimension, L_x and L_y. More specifically, since we add incomplete unit cells to complete the lattice, L_i will give us the number of plaquettes (a square with eight atoms and one hole in the middle). This way the coordinates will range from $-L_i$ to L_i, with the origin at the center of the lattice. To have a more symmetrical lattice, we will use $L_x = L_y = L$. Each atom is connected to its neighbours. In this picture, the lattice of atoms is an undirected graph. We now consider the problem of adding an electron to the lattice. We can associate to each site (atom) a state, $|x, y\rangle$. If the state of the electron is $|\Psi\rangle = |x, y\rangle$ then the electron is located at that site. The electron state can, of course, spread over several sites. Neighbouring atoms are connected, meaning the electron can jump from

site to site through these connections. Let us denote the rate of transfer of wave function amplitude from a site i to j (more simply, the hopping parameter) by h_{ij}. We use the notation of h instead of the usual t to differentiate from time, although this is not very important since we will soon remove this parameter. We will assume h_{ij} is equal for all connections, $h_{ij} = h$. For example, the evolution over time of the wave function amplitude $\Psi_{x,y}$ at a B site will be,

$$i\frac{d\Psi_{x,y}}{dt} = -h\Psi_{x-1,y} - h\Psi_{x+1,y}. \tag{2.1}$$

where $\Psi_{x\pm1,y}$ are the amplitudes at the neighbouring sites. We have analogous equations for all sites. In Eq. 2.1, the hopping parameter can be absorbed into the time by $t' = -ht$, so the hopping parameter only sets a time scale in the evolution of a state. The time evolution equation is

$$i\frac{d\left|\Psi\right\rangle}{dt} = \hat{H}\left|\Psi\right\rangle, \tag{2.2}$$

so we can extract the (tight-binding) Hamiltonian from these equations:

$$\hat{H} = \sum_{x=-L,2}^{L}\sum_{y=-L}^{L-1}\left|x,y+1\right\rangle\left\langle x,y\right| + H.c. + \sum_{y=-L,2}^{L}\sum_{x=-L}^{L-1}\left|x+1,y\right\rangle\left\langle x,y\right| + H.c.\ . \tag{2.3}$$

Here we have already removed the hopping parameter. The first sum in each term is done with a step of two, indicated by $(,2)$, to skip the lines with holes. The first term is a sum of upward and downward hopping terms, where the downward terms are the Hermitic conjugate of the upward terms, while the second is a sum of horizontal hopping terms. We can see again a relation with graphs, since $\hat{H}$ became equal to the adjacency matrix of the lattice with our choices of parameters. In the presence of a potential energy $V(\boldsymbol{r},t)$, we would introduce that potential in the diagonal elements of the Hamiltonian, known as the on-site potentials, $\left\langle x,y\right|\hat{H}\left|x,y\right\rangle = V(x,y,t)$. Even if there is no potential, the energies are always defined up to a constant of our choice, so we can add a constant potential ϵ_0 to the Hamiltonian.

Since we considered a state per atom of the lattice, our basis of states has size $(2L+1)^2$. We simply assumed it is possible to build such a basis, but, to make sure this model has physical significance, an important question to ask is, is there a basis of orthonormal states where each state is heavily localized at an atom? The atomic orbitals are localized at each atom, but they are not orthogonal to each other. The answer to the question is, yes, there is, and the basis in question is the Wannier basis. The eigenstates of the crystalline Hamiltonian will be Bloch states. We can transform the Bloch basis by a Fourier transformation to obtain the Wannier basis. While the Bloch states span the whole lattice, the Wannier states are fairly localized at specific atoms, and, in the limit of $h \to 0$ (isolated atoms), they become atomic orbitals. The Wannier basis is localized and orthonormal, but there are infinite Wannier states for each atom while in our model there is only one state per atom. Still, we can consider our electron has a low enough energy so that only Bloch states composed of the lowest energy unoccupied Wannier states are in reach. In this case, we can consider there is only one state per site, with $\left|x,y\right\rangle$ being the lowest energy unoccupied Wannier state of the atom at (x,y).

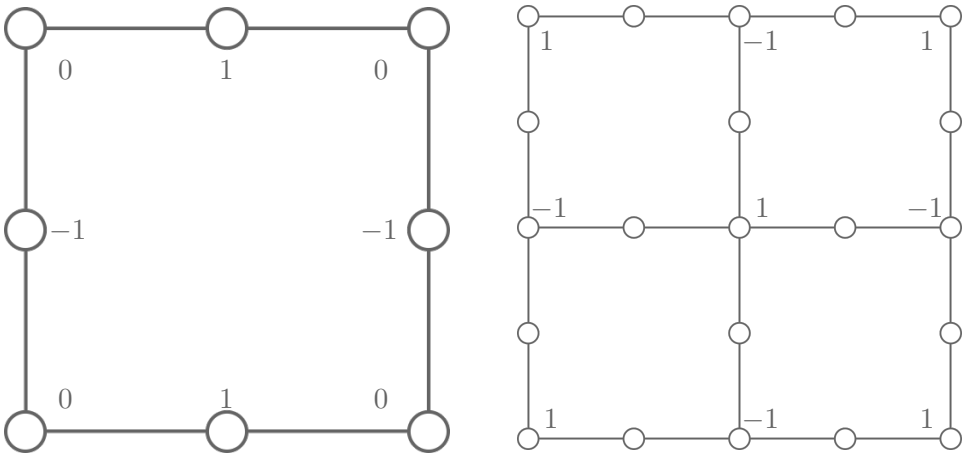

(a) One-plaquette localized state. (b) Zero energy itinerant state.

Figure 2.2: Zero energy eigenstates (not normalized) of the tight-binding Hamiltonian.

2.2 Zero energy eigenstates

The Lieb Hamiltonian, Eq. 2.7, has a degenerate flat band containing states that spread over the whole lattice when written in their momentum form, but we can combine these states to form localized states $|L\rangle$ (which are eigenstates of zero energy) that occupy a small region of the lattice and continue to be eigenstates when we increase the size of the lattice. The most compact form of a localized state occupies only one plaquette (Fig.2.2a). This state has finite amplitude at B and C sites, being zero at A sites. The electron is locked in a localized state by destructive interference with itself. If we write the time evolution equation at a nearby A site,

$$i\frac{d\Psi_A}{dt} = \Psi_B + \Psi_C = 1 - 1 = 0. \tag{2.4}$$

The same is true for any site. The whole state will not evolve over time: it is a zero energy eigenstate. We can place a one-plaquette localized state in each of the L^2 plaquettes. The number of localized states is equal to the number of plaquettes, but neighbouring one-plaquette localized states are not orthogonal, so they form a non-orthogonal sub-basis. They do do not form a basis of the zero energy subspace because there is one zero energy state that is not localized. This state spans all A sites (Fig. 2.2b) and nearby A sites interfere destructively. We can not reduce the size of the state, neither would the state stay contained if we increased the size of the lattice: the state would leak out by the outer A sites, which is why localized states do not have component in A sites.

Important to note this basis of the zero energy subspace we just considered is just a choice. Any other linearly independent combination would do. We will even see later this is not the most convenient basis because of how the magnetic field reduces the degeneracy of this subspace.

2.3 Introduction of magnetic field

The Hamiltonian of a particle of mass $m = 1$ and charge $q = 1$ (even though we are thinking of an electron) in the presence of a magnetic field $\boldsymbol{B} = \nabla \times \boldsymbol{A}$ with vector potential $\boldsymbol{A}$ is

$$\hat{H} = \frac{1}{2}(i\nabla + \boldsymbol{A})^2, \tag{2.5}$$

assuming $\hbar = 1$. Whenever the particle travels along a line L, the electron suffers a phase change given by

$$\exp\left(i \int_L \boldsymbol{A} \cdot d\boldsymbol{r}\right), \tag{2.6}$$

so the angle is given by the line integral of $\boldsymbol{A}$ along line L. This is called the Peierls phase. It is taken into account by multiplying the hopping parameters by this term, where the path of integration will be the straight lines that connect neighbours. This is called the Peierls substitution.[24] Our tight-binding Hamiltonian becomes

$$\begin{aligned} \hat{H} = &\sum_{x=-L,2}^{L} \sum_{y=-L}^{L-1} \exp\left(i \int_{x,y}^{x,y+1} \boldsymbol{A} \cdot d\boldsymbol{r}\right) |x, y+1\rangle \langle x, y| + H.c. \\ &+ \sum_{y=-L,2}^{L} \sum_{x=-L}^{L-1} \exp\left(i \int_{x,y}^{x+1,y} \boldsymbol{A} \cdot d\boldsymbol{r}\right) |x+1, y\rangle \langle x, y| + H.c. \ . \end{aligned} \tag{2.7}$$

We could question our choice of path, since the electron can go from one atom to another through an infinite number of paths. We could consider, for example, that it is easier for the electron to go from one atom to another along a curved, arc-like path, since its trajectories are naturally curved while moving in a magnetic field. The problem with this is, if the electron were to travel slowly turning to one side when going from atom i to j, then when it returned from j to i it would do so along a different, reflected path and the phase in one direction would not be minus the phase of the inverse direction, as required by the hermitian property of the Hamiltonian, because there will be a magnetic flux inside the area limited by both curves. Choosing the same curved line for both directions would not be right because of lack of symmetry, so the straight line is actually the only possible choice.

To be completely precise, we would have to consider an integration over all possible paths, and also remember that the electron is never perfectly localized at one point, but that would diverge too much from the scope of this thesis. Suffice it to say, in this model, the electron is *tightly bound*, not only to the atoms, but also in the paths it can take from atom to atom. Of course, we can always perform a change of the lattice basis by multiplying each state by a phase in such a way as to modify or even remove several hopping phases. For example, the following transformation,

$$|x_2, y_2\rangle \to \exp\left(-i \int_{x_1,y_1}^{x_2,y_2} \boldsymbol{A} \cdot d\boldsymbol{r}\right) |x_2, y_2\rangle, \tag{2.8}$$

results in

$$\exp\left(i\int_{x_1,y_1}^{x_2,y_2}\boldsymbol{A}\cdot d\boldsymbol{r}\right)|x_2,y_2\rangle\langle x_1,y_1| \to |x_2,y_2\rangle\langle x_1,y_1|\,. \tag{2.9}$$

This does not mean we can remove all the phases entirely, removing the magnetic field. We could only do so if there were no loops on our lattice. Since there are loops, then there is also a magnetic flux inside those loops:

$$\oint_{\partial S}\boldsymbol{A}\cdot d\boldsymbol{r} = \iint_S \boldsymbol{B}\cdot d\boldsymbol{S}. \tag{2.10}$$

Since the right term is gauge invariant the left term will be too. We can attribute phases to the hopping terms in many different ways, as long as Eq.2.10 is respected. However, since we will increase the magnetic field over time, to remove phases we would need a time dependent gauge transformation, making our basis of states time dependent. Since it is easier to work with a time independent basis of states, we shall use $\hat{H}$ as in Eq. 2.7.

2.4 Localized states with magnetic flux

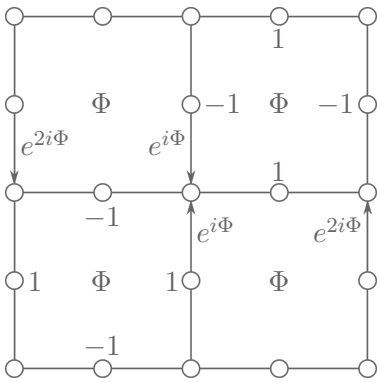

Figure 2.3: In the atoms: two plaquette localized state. In the plaquettes: flux in each plaquette. In the arrows: phase gained in a jump on that direction.

When we add magnetic field, the one-plaquette localized states are no longer eigenstates. To see this, consider our gauge has only one or two jumps with phase per plaquette (Fig. 2.3). Let us try to build a localized state on the bottom-left plaquette of the figure. Since we can define a state up to a global phase, we can set a value of 1 at a given atom, for example, the right C site. To have destructive interference, the bottom B site must be -1. Continuing in this direction around the loop, the left C site will be 1 and the top B -1, but then, when we return to the initial atom, the flux phase change in the last step will not allow us to properly close the loop of destructive interference. The solution is to continue to the right of the top B site and perform a loop in the opposite direction around the top-right plaquette and only then close in the initial atom. This way, the flux phase of each plaquette will cancel. This diagonal state is then localized for any value of flux. A one-plaquette localized state can be interpreted as a standing wave in a ring. A two-plaquette localized state can be interpreted as a standing wave in a larger ring that was twisted to form two smaller rings.[5]

In a basis with only one or two jumps with phase per plaquette, the Hamiltonian can be written with only jumps of phase Φ or multiples of it, which implies a periodicity of $\Phi = 2\pi n$ of the Hamiltonian matrix, and consequently a periodicity of the energies. Using a more general gauge, the energies will still have the same periodicity but the Hamiltonian eigenbasis may not be periodic.

2.5 Positive-negative energy symmetry

Without flux there are L^2 localized states and one itinerant state in the zero energy subspace (itinerant state can be defined simply as a non-localized state). When we add flux, the degenerate subspaces usually break into individual states that differentiate in energy. This will not happen to the flat band of the Lieb lattice and the bipartite property of the Lieb lattice can be used to justify this.

Consider the change of lattice basis $\{|\mathrm{BC}\rangle \to -|\mathrm{BC}\rangle\}$, meaning a change of sign at all the BC sites. Since the Hamiltonian consists of only jumps between A and BC sites, the change of basis will change the sign of all jumps, $\{\hat{H} \to -\hat{H}\}$. We may define an operator for this transformation through its application in the lattice states,

$$\hat{T}_{BC}\,|x,y\rangle = (-1)^{x+y}\,|x,y\rangle\,. \tag{2.11}$$

Consider two states related by the BC to minus BC transformation:

$$\begin{aligned} |E_+\rangle &= \frac{1}{\sqrt{2}}(|A\rangle + |BC\rangle), \\ |E_-\rangle &= \frac{1}{\sqrt{2}}(|A\rangle - |BC\rangle), \end{aligned} \tag{2.12}$$

where we separated the component of each state in the A and BC sub-lattices. Consider $|E_+\rangle$ is an eigenstate with energy E_+:

$$\hat{H}\,|E_+\rangle = E_+\,|E_+\rangle\,. \tag{2.13}$$

Using the BC to minus BC transformation:

$$\begin{aligned} \hat{T}_{BC}\hat{H}\hat{T}_{BC}\hat{T}_{BC}\,|E_+\rangle &= E_+\hat{T}_{BC}\,|E_+\rangle\,, \\ -\hat{H}\,|E_-\rangle &= E_+\,|E_-\rangle\,, \end{aligned} \tag{2.14}$$

we conclude $|E_-\rangle$ is also an eigenstate with energy $E_- = -E_+$. For every non-zero energy state there is a state of opposite energy given by a BC to minus BC (or A to minus A) transformation of the other. We can derive from here another property:

$$\begin{aligned} &\langle E_+|E_+\rangle = 1,\ \ \langle E_+|E_-\rangle = 0, \\ \implies &\langle A|A\rangle = \langle BC|BC\rangle = 1. \end{aligned} \tag{2.15}$$

This means the itinerant state of the flat band that spans all A sites (Fig. 2.2b) does not leave the flat band alone, it must mix with a localized state to form two opposite energy states. Also, since that state is the only one of the flat band with a component in A sites, only two states may leave the flat band. The combination of the two factors, localized states not having component in A sites, and non-zero energy states requiring a component in A sites, do not allow the flat band to break apart with the magnetic field, apart from a single localized state and the itinerant state that are lost.

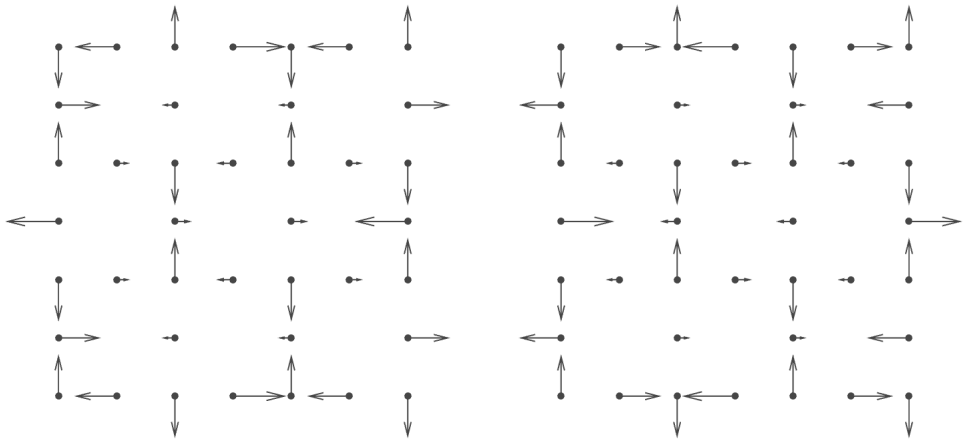

(a) S_-. (b) S_+.

Figure 2.4: S states of a 3×3 lattice at $\Phi = 0$. The value of the wave function at each site is represented as a vector in the complex plane.

We show in section 2.7 that two states leave the flat band when we add magnetic flux. We shall refer to these two states as S states ($|S_\pm\rangle$). The S states at zero flux are shown in Fig. 2.4. The value of the wave function at a site is represented as a vector in the complex plane. The S states lie in each vertex of the itinerant bands, at $\boldsymbol{k} = (\pi, \pi)$. They are a combination of the (π, π) itinerant state and the (π, π) localized state. When we introduce flux a gap appears between itinerant bands. A k_x (k_y) of π means a phase change of π from a unit cell to the next in the x (y) direction, or, equivalently, a $\pi/2$ phase change from site to site, as seen in the figure. The A sites are all occupied with the same probability, while BC occupation increases as we move away from the center of the lattice, so the S states could be considered edge states, or at least their components in the BC sub-lattice could be. This is no longer true for larger values of flux.

2.5.1 Eigenstates of the squared Hamiltonian

As a side note from the main focus of this thesis, the bipartite property of the lattice has an interesting consequence on $\hat{H}^2$. Consider a state of energy E, $|E\rangle = (|A\rangle + |BC\rangle)/\sqrt{2}$. We may write the eigenvalue equation as

$$(\hat{H}\,|A\rangle + \hat{H}\,|BC\rangle)/\sqrt{2} = (E\,|A\rangle + E\,|BC\rangle)/\sqrt{2}. \tag{2.16}$$

Since $\hat{H}$ only connects A to BC sites, $\hat{H}\,|A\rangle$ ($\hat{H}\,|BC\rangle$) is a state in the BC (A) sub-lattice, so we may separate 2.16 in to two equations:

$$\begin{aligned} \hat{H}\,|A\rangle &= E\,|BC\rangle\,, \\ \hat{H}\,|BC\rangle &= E\,|A\rangle\,. \end{aligned} \tag{2.17}$$

From here we can deduce that, if $|\Psi\rangle$ is an eigenstate of zero energy with components in both sub-lattices, then $|A\rangle$ and $|BC\rangle$ are also zero energy eigenstates. We conclude that

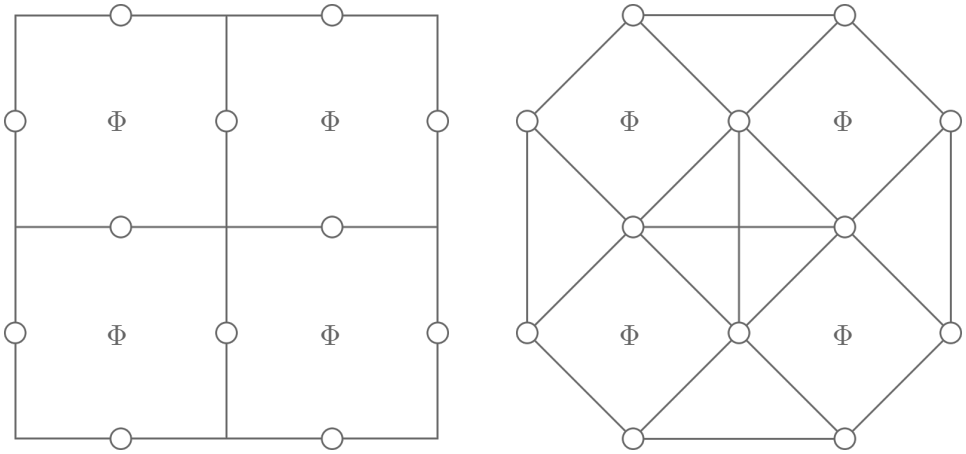

(a) (b)

Figure 2.5: (a) 2×2 BC Lieb sub-lattice. (b) BC sub-lattice with straight connections. It is a Mielke lattice.

we may separate the zero energy subspace into two group of states, each belonging to only one of the sub-lattices. By multiplying by $\hat{H}$ we may decouple the equations into

$$\begin{aligned} \hat{H}^2 |A\rangle &= E^2 |A\rangle , \\ \hat{H}^2 |BC\rangle &= E^2 |BC\rangle , \end{aligned} \tag{2.18}$$

so $|A\rangle$ and $|BC\rangle$ are eigenstates of $\hat{H}^2$, which is still the Hamiltonian of a tight-binding system. More specifically, $\hat{H}^2$ contains the Hamiltonians of two independent tight-binding systems with hopping constants h^2. Since $\hat{H}$ has only nearest neighbour hoppings, $\hat{H}^2$ will have only second to nearest neighbours jumps, but, with only second jumps, from an A site we jump to an A site, and from a BC we jump to a BC, so both sub-lattices, A and BC, are decoupled, just like in the equations 2.18. Since with two consecutive jumps we can also jump to a neighbour and then return to the original site, an on-site potential also appears, of value nh^2, where n is the number of neighbours of each site, so we have $4h^2$ in A sites and $2h^2$ in BC sites.

We may separate (block diagonalize) $\hat{H}^2$ in to two new Hamiltonians, each pertaining to a new lattice. The lattice of A sites is a regular square lattice. The lattice of BC sites is of the Mielke-type[3] (Fig. 2.5a). In the Mielke-type lattice, jumps from B to B and C to C are performed in a straight line, while B to C jumps go through the A site that connected them. For a constant flux we may change the shape of the connections to fit the usual picture of the Mielke lattice (Fig. 2.5b), as long as we do not change the flux in each plaquette. The flux in plaquettes with the + connections is always zero. This was needed to keep the flat band flat with the introduction of flux, since the usual Mielke lattice does not have a flat band with flux.

In short, we can say of a Lieb eigenstate $|E\rangle$ that if $E = 0$ then the state is either a zero energy eigenstate of the A sub-lattice or of the BC sub-lattice. If $E \neq 0$, then

$|E\rangle = (|A\rangle + |BC\rangle)/\sqrt{2}$, where $|A\rangle$ ($|BC\rangle$) is an eigenstate of the A (BC) sub-lattice of energy E^2. The A sub-lattice is a regular square lattice with $\epsilon_0 = 4h^2$ and the BC sub-lattice is a Mielke lattice with $\epsilon_0 = 2h^2$ and no flux in plaquettes with + connections.

This is the perspective of deconstruction of the Lieb lattice. The inverse perspective, construction of the Lieb lattice from the combination of both lattices, is also true. Consider a square lattice with $\epsilon_0 = 4h^2$, where h^2 is the hopping constant, and a Mielke lattice with $\epsilon_0 = 2h^2$ (with flux only in the empty plaquettes), both with the same size. Both lattices have an itinerant band. The on-site potentials will equalize the energy dispersion relations of both bands. At zero flux, the energies are

$$\begin{aligned} E_{SM} &= 4h^2 + 2h^2[\cos(k_x) + \cos(k_y)] \\ &= 4h^2[\cos(k_x/2)^2 + \cos(k_y/2)^2]. \end{aligned} \tag{2.19}$$

Each pair of same energy states will combine to create the Lieb eigenstates:

$$|E_\pm\rangle = (|E_{SM}\rangle_S \pm e^{i\theta} |E_{SM}\rangle_M)/\sqrt{2}, \tag{2.20}$$

of energies $E_\pm = \pm\sqrt{E_{SM}}$, for some θ. The zero energy subspace will be the reunion of the subspaces of both lattices. The Mielke-type lattice has a zero energy band of localized states that the Lieb lattice inherits directly.

2.6 Rotation and reflection invariance of the eigenstates

Our physical system consists of a square-like lattice in a uniform perpendicular magnetic field. The point group symmetries of this system apply directly to the probability density of the eigenstates. The eigenstates themselves will only be invariant under the symmetry operations if the vector potential also is. The symmetry of the system is represented by the C_4 cyclic group. It is a rotational symmetry around an axis in the middle of the lattice, $|\Psi_{x,y}|^2 = |\Psi_{-y,x}|^2 = |\Psi_{-x,-y}|^2 = |\Psi_{y,-x}|^2$, so the wave function at two sites $\pi/2$ one from the other will only differ from a phase, $\Psi_{-y,x} = e^{i\theta}\Psi_{x,y}$. If we choose a gauge that is also rotationally symmetric, $\boldsymbol{A} \propto (-y, x)$, then all four $\pi/2$ jumps are equivalent, so the phase gained will be the same for all jumps. Jumping $\pi/2$ four times around the lattice, we must return to the same wave function value, meaning $e^{4i\theta} = 1 \leftrightarrow e^{i\theta} = u_4 = 1, -1, i, -i$. The exception to the rule are the localized states due to the fact that they are part of a degenerate subspace, but there is a basis of states of the flat band where all the states are invariant up to a phase under a C_4 rotation. States with $u_4 = \pm 1$ will be equal in opposite sites of the lattice, while states with $u_4 = \pm i$ will have opposite signs, so we may call the first ones *even* and the latter ones *odd*.

We may express the rotational symmetries analytically using a rotation operator. Consider the $+\pi/2$ rotation operator, $\hat{R}_{\pi/2} |x, y\rangle = |-y, x\rangle$ and the eigenstate $|E\rangle$. Then

$$\begin{aligned} \hat{H}(\Phi) |E(\Phi)\rangle &= E |E(\Phi)\rangle , \\ \hat{R}_{\frac{\pi}{2}} \hat{H}(\Phi) \hat{R}_{-\frac{\pi}{2}} \hat{R}_{\frac{\pi}{2}} |E(\Phi)\rangle &= E \hat{R}_{\frac{\pi}{2}} |E(\Phi)\rangle , \\ \hat{H}(\Phi) \hat{R}_{\frac{\pi}{2}} |E(\Phi)\rangle &= E \hat{R}_{\frac{\pi}{2}} |E(\Phi)\rangle , \end{aligned} \tag{2.21}$$

so $\hat{R}_{\pi/2}|E\rangle$ is also an eigenstate of energy E. If the eigenspace of energy E has only one state, then $\hat{R}_{\pi/2}|E\rangle$ must give us $|E\rangle$, apart from a phase. If the eigenspace has more than one state, then we may obtain one of the other states of the eigenspace. For example, we can see in Fig. 2.4 that the S states have $u_4 = -1$ on a 3×3 lattice. It is easy to check that if a state has a $\pi/2$ phase difference between nearest neighbours then it is even, with $u_4 = (-1)^L$.

At $\Phi = 0$, the symmetry of the system is C_{4v}, which incorporates the reflections σ on the x, y axes and on the diagonals. For non-zero flux the reflections are not proper transformations. In a symmetric gauge, $\boldsymbol{A} \propto (-y, x)$, a reflection will change the sign of A, or equivalently, $\Phi \to -\Phi$. Using a reflection operator $\hat{R}_\sigma$,

$$\begin{aligned} \hat{R}_\sigma \hat{H}(\Phi)\hat{R}_\sigma \hat{R}_\sigma |E(\Phi)\rangle &= E\hat{R}_\sigma |E(\Phi)\rangle\,, \\ &= \hat{H}(-\Phi)\hat{R}_\sigma |E(\Phi)\rangle = E\hat{R}_\sigma |E(\Phi)\rangle\,, \end{aligned} \tag{2.22}$$

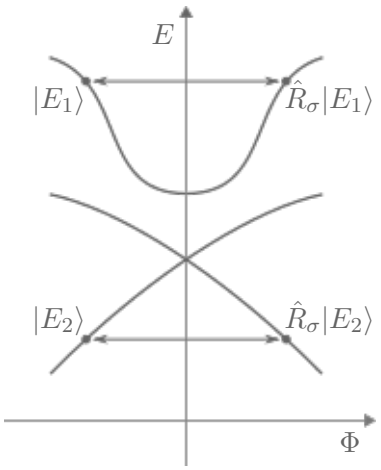

Figure 2.6: Energies of, on top, a σ invariant state at $\Phi = 0$ and, below, a pair of states related by reflection.

so $\hat{R}_\sigma |E(\Phi)\rangle$ is an eigenstate of the lattice with flux $-\Phi$. For $\Phi = 0$ there is a basis where all states are invariant under C_{4v} operations, but the basis with degeneracy broken by the flux $\{|E(\Phi)\rangle\}, \Phi \to 0$ will not be that basis. Although the states are C_4 invariant for any flux, only some will be σ invariant at zero flux. For a state $|E(\Phi)\rangle$ where $\hat{R}_\sigma |E(0)\rangle = u_\sigma |E(0)\rangle$, the changes of flux $+\Delta\Phi$ and $-\Delta\Phi$ starting from $\Phi = 0$ are equivalent, which means $E(\Phi)$ is even. If the state is not σ invariant, the energies of the state and its reflection are reflections on $\Phi = 0$ one of the other (Fig. 2.6).

Some eigenstates will be C_{4v} invariant at $\Phi = 0$, meaning $E_{-x,y} = u_\sigma E_{x,y}$ (and others), and $E_{-y,x} = u_4 E_{x,y}$. If we choose a diagonal site, where $x = y$, from the comparison of both equations we will conclude that $u_4 = u_\sigma$, so a state that is σ invariant is even, unless the state is zero at all the diagonal sites, which are A sites, so the localized states do not have to follow this relation. It has been found numerically that all the even itinerant states are σ invariant at $\Phi = 0$ and all the odd ones are not, except for the two S states, which are even but not σ invariant. The S states are in a unique position in that they combine two symmetries already discussed: the $\pm E$ symmetry and the $\pm\Phi$ symmetry. Using the reflection relation between both S states and separating it in an equation for each sub-lattice,

$$\hat{R}_\sigma |S_+(\Phi)\rangle = u\,|S_-(-\Phi)\rangle\,, \tag{2.23}$$

$$\hat{R}_\sigma(|A(\Phi)\rangle + |BC(\Phi)\rangle) = u(|A(-\Phi)\rangle - |BC(-\Phi)\rangle), \tag{2.24}$$

$$\hat{R}_\sigma |A(\Phi)\rangle = u\,|A(-\Phi)\rangle\,, \tag{2.25}$$

$$\hat{R}_\sigma |BC(\Phi)\rangle = -u\,|BC(-\Phi)\rangle\,. \tag{2.26}$$

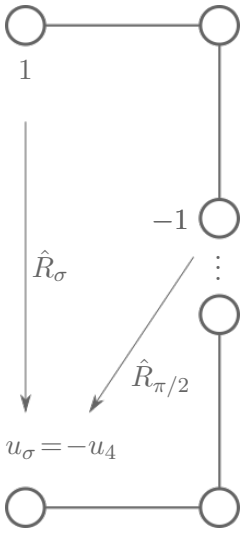

Figure 2.7: Invariance relation of localized states.

we find out each sub-lattice state will be σ invariant at $\Phi = 0$, with opposite invariance phases $\pm u$. It is possible to determine u. Considering the A state (Fig. 2.2b) in an $L \times L$ lattice, it is easy to check that the reflection phase of the A state is $u_\sigma = u = (-1)^L$, and so for the BC state we have $u_\sigma = -u = (-1)^{L+1}$. As a reminder, the rotation phase of the S states, and therefore of both sub-lattice states, is $u_4 = (-1)^L$.

At $\Phi = 0$, there is a basis of states of the localized subspace where all states are C_{4v} invariant. The rotation and reflection constants u_4 and u_σ of each state will be related. Consider the A site at a corner of a localized state, who connects a B to a C site (Fig. 2.7). If the state is 1 at the B site, then, being at the corner, it must be -1 at C. Applying both symmetry operations to the next corner we find that $u_\sigma = -u_4$. One of the consequences of this is that the base with both symmetries well defined has no states with $u_4 = \pm i$. The BC state of the S states is also a localized state at $\Phi = 0$ and follows the same relation $u_\sigma = -u_4$, as we can check above.

2.7 Energy diagram with magnetic flux

In Fig. 2.8a we have the energies of an 8×8 ($L = 8$) Lieb lattice as a function of the magnetic flux. Up to now we thought of the flat band mainly in terms of its zero flux characteristics: L^2 localized states and one itinerant state. Since from now on we will always consider the possibility of flux being present, zero flux becomes only a particular case in a more general situation. It will make more sense to divide the eigenstates in three groups: the flat band, consisting of the $L^2 - 1$ localized states; two S states, whose energies cross the flat band at $\Phi = 2\pi n$, the crossing points; the itinerant bands, one upper band, and a lower band symmetrical to the upper band.

In contrast with other decorated lattices, the Lieb lattice is different in that there is still a flat band when we apply a magnetic field. The energies of each itinerant band intertwine in a fractal-like pattern called Hofstadter's butterfly.[25] All states remain in their bands, upper, lower, or flat, except for the two S states, not being possible to assign them a band. As we increase the flux, the S states cross the flat band, intertwine with states in one itinerant band, then cross again to intertwine with the other band in a symmetrical way (Fig. 2.8b).

In square Lieb lattices, the highest and lowest energy parts of the itinerant bands separate from the bulk of states in sub-bands of four states (Fig. 2.8c), one of each type of C_4 invariance $\pm 1, \pm i$. The larger the lattice, the more four-state sub-bands there are. The four states seem entwined like threads in rope. The sub-bands of exception are the closest to the flat band in each itinerant band: each contains three states that never leave their respective itinerant bands, but both exchange the two S states at each crossing point.

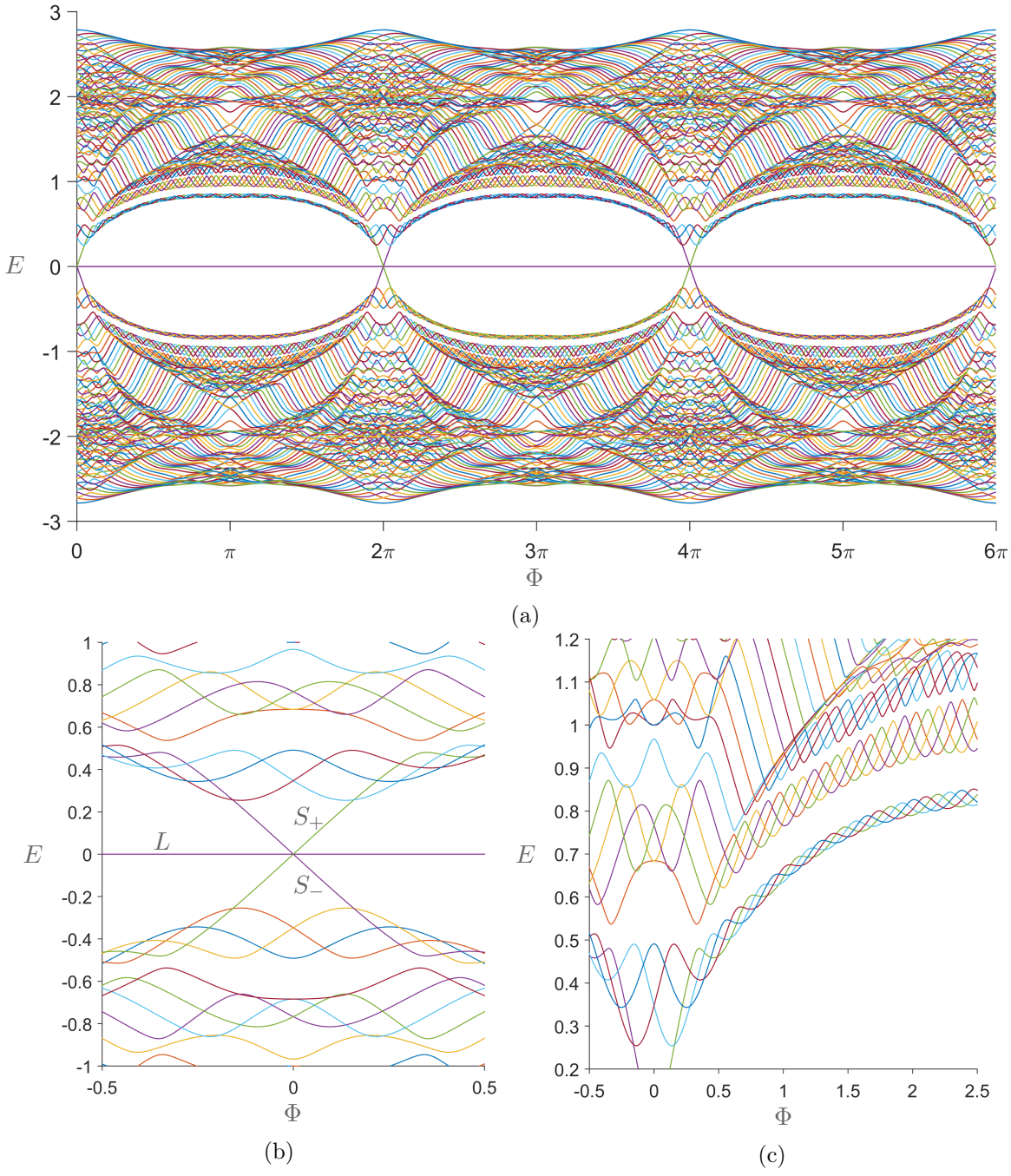

Figure 2.8: (a) Energy flux diagram of an 8×8 Lieb lattice. The zero energy subspace is degenerate. Note the periodic energy crossings at $\Phi = 2\pi n$. (b) Close-up of the region where the S levels cross the flat band. (c) Itinerant band four-state sub-band structure.

2.7.1 Numerical ordering of eigenstates

Fig. 2.8 was obtained by numerically diagonalizing the Hamiltonian for many values of flux using MATLAB.[26] It is noticeable by the color of the lines in the figures that the energies are ordered. For each flux the numerical method gives us a list of energies and states, but we do not know how they are related with the energies and states of neighbouring fluxes. It is expected that the energy functions $E_i(\Phi)$ (and the states $|E_i(\Phi)\rangle$) are continuous and differentiable in Φ, so we may use this to order the numerical data. For example, consider two sets of states $\{|E_i(\Phi)\rangle\}$ and $\{|E_j(\Phi + d\Phi)\rangle\}$. We may order the second set using the products $|\langle E_i(\Phi)|E_j(\Phi + d\Phi)\rangle|^2$: for each state i, the state j that gives the maximum value of the dot product will be the matching state. In practice, this method sometimes failed at points where energies met, so higher order methods were used to improve precision. The ordering is needed to calculate numerically the derivative with respect to the flux of a state or of the energies, for example.

Another thing to note is the phase coherence of the states obtained numerically. The diagonalization method may give us a list of (assuming ordered) states $\{|E_i(\Phi_n)\rangle\}$ with random phases multiplied to each state and at each flux due to the gauge freedom. To guarantee phase coherence we may divide each state (i, n) by their phase at a site $|x, y\rangle$, so that all states have the same phase, zero, at the same lattice site.

Chapter 3

Time evolution in the Lieb lattice

In this chapter, we study the importance of the choice of vector potential in time dependent systems, present a general time evolution formalism and, one by one, we introduce properties of the Lieb lattice into the equations to obtain several properties of the time evolution.

3.1 Vector Potential

The choice of vector potential $\boldsymbol{A}$ is never unique: for our case of $\boldsymbol{B} = (0, 0, B(t))$, the most general vector potential is

$$\boldsymbol{A} = B(t)(-ay, (1-a)x) + \nabla f(\boldsymbol{r}, t). \tag{3.1}$$

We omit the third dimension since it is not relevant to our 2D lattice. If there is an electric potential, we may absorb it into $\boldsymbol{A}$ such that the vector potential will give us the full electric field $\boldsymbol{E} = -\partial \boldsymbol{A}/\partial t$. The electric potential will be related with f. For any a and any function f, the magnetic field is the same, but the electric field is not:

$$\boldsymbol{E} = -\frac{\partial B}{\partial t}(-ay, (1-a)x) - \nabla \frac{\partial f}{\partial t}, \tag{3.2}$$

which means our choice of a and f will depend on the electric field, which in turn depends on the geometry of the source of magnetic field. Let us consider our source is an infinite solenoid, centred at $\boldsymbol{r}_0 = (x_0, y_0)$, with the lattice inside it, at $(0, 0)$. Since there is a rotational symmetry around $\boldsymbol{r}_0$, $\boldsymbol{A}$ is invariant under rotations around $\boldsymbol{r}_0$:

$$\boldsymbol{A} = \frac{B(t)}{2}(-(y-y_0), x-x_0) + \nabla f(r, t), \tag{3.3}$$

where r is the distance to the axis of the solenoid. Applying Gauss's law to determine f we obtain $\nabla f(r, t) = 0$, so we end up with

$$\boldsymbol{A} = \frac{B(t)}{2}[(-y, x) + (y_0, -x_0)], \tag{3.4}$$

$$\boldsymbol{E} = \frac{1}{2}\frac{\partial B}{\partial t}[(y, -x) + (-y_0, x_0)]. \tag{3.5}$$

Both fields $\boldsymbol{A}$ and $\boldsymbol{E}$ are circular and invariant under rotations around (x_0, y_0). Both fields can also be divided into a circular component invariant under rotation around the center of the lattice $(0, 0)$, together with a uniform field pointing towards $\pm(-y_0, x_0)$, so the two following physical situations seem related: (a) with the solenoid centred at (x_0, y_0), we change $\boldsymbol{B}$ over time, or (b) with the solenoid centred at (0,0), we change $\boldsymbol{B}$ while also applying a uniform electric field in the $(-y_0, x_0)$ direction. In practice, we will simulate the situation (a), but the results are still applicable to cover situation (b).

3.1.1 Length and velocity gauges

The Schrödinger equation of a particle using atomic units in a uniform electric field $\boldsymbol{E}(t)$ is

$$i\frac{\partial \Psi}{\partial t} = \left(-\frac{\nabla^2}{2} - \boldsymbol{r}\cdot\boldsymbol{E}(t)\right)\Psi(\boldsymbol{r}, t). \tag{3.6}$$

This is called the Schrödinger equation in the length gauge.[27] Just like in the previous section, we should be able to absorb the electric potential $-\boldsymbol{r}\cdot\boldsymbol{E}(t)$ into a vector potential by a gauge transformation. That gauge transformation is

$$\Psi \to \exp\left(i\boldsymbol{r}\cdot\int_0^t \boldsymbol{E}dt'\right)\Psi. \tag{3.7}$$

Substituting in 3.6 we obtain the Schrödinger equation in the velocity gauge,

$$i\frac{\partial \Psi}{\partial t} = \frac{1}{2}\left(i\nabla - \int_0^t \boldsymbol{E}dt'\right)^2\Psi(\boldsymbol{r}, t), \tag{3.8}$$

where we may define $\boldsymbol{A} = -\int_0^t \boldsymbol{E}dt'$ so that $\boldsymbol{E} = -\partial\boldsymbol{A}/\partial t$. The time evolution of a state is equal in both gauges, apart from a gauge transformation. More importantly, the gauge transformation will not alter inner products, so the projection of the state in the localized subspace over time will be the same in both gauges and our results will be general to both the (a) and (b) situations in section 3.1. Note, however, that the eigenstates of the Hamiltonian in each gauge are different. For example, while the localized states form a degenerate zero energy subspace of $\hat{H}$ for the velocity gauge, the electric potential of the length gauge will break the degeneracy of the flat band, so to study the evolution of the localized states it is better to use the gauge where they are eigenstates, the velocity gauge.

3.1.2 Final fields

To finalize the discussion regarding the fields, we still need to specify the time dependence of the magnetic field. More specifically, we are interested in the magnetic flux $\Phi(t) = B(t) \times (\text{Area of plaquette}) = 4B(t)$. We shall consider the most simple case, a linear dependence with time, $\Phi(t) = \omega t$. We choose ω as our constant because in our system of units the flux is an angle, so ω is an angular frequency. The vector potential becomes

$$\boldsymbol{A} = \frac{\omega t}{8}(-(y - y_0), x - x_0) = \frac{\omega t}{8}(-y, x) - \boldsymbol{E}_0 t, \tag{3.9}$$

where $\boldsymbol{E}_0 = \omega(-y_0, x_0)/8 = r_0\omega(\cos\alpha, \sin\alpha)/8$, $r_0 = \sqrt{x_0^2 + y_0^2}$ is a uniform electric field. ω controls the intensity of both components of electric field, although the uniform component has an additional degree of freedom for its intensity, r_0.

What appears in the Hamiltonian are path integrals of the fields and not the fields directly (Eq. 2.7). The Peierls angle on a jump from (x, y) to $(x + \Delta x, y + \Delta y)$ is

$$\int_{x,y}^{x+\Delta x, y+\Delta y} \boldsymbol{A} \cdot d\boldsymbol{r} = \frac{\omega t}{8} \left(-(y - y_0)\Delta x + (x - x_0)\Delta y\right). \tag{3.10}$$

For nearest neighbour jumps we have $(\Delta x, \Delta y) = (\pm 1, 0)$ or $(0, \pm 1)$.

3.2 Evolution in the Hamiltonian eigenspace

The quantity we are interested in is $|\Psi_0(t)|^2 = \sum_i |\langle \Psi(t) | L_i(t) \rangle|^2$, where we sum over all localized eigenstates of a time dependent Hamiltonian. It will be useful to use as basis of states at time t the eigenstates of $\hat{H}(t)$. Let us consider a quantum system with a time dependent, discrete, Hamiltonian,

$$i\frac{d\,|\Psi\rangle}{dt} = \hat{H}(t)\,|\Psi\rangle\,. \tag{3.11}$$

We may write this equation in a time independent basis of states, $\{a\}$,

$$i\frac{d\boldsymbol{\Psi}_a}{dt} = H_a(t)\boldsymbol{\Psi}_a. \tag{3.12}$$

where $\boldsymbol{\Psi}_a$ is the column vector of Ψ in the basis $\{a\}$. This basis may be, for example, the basis of lattice sites $|x, y\rangle$. Consider now the basis of eigenstates of $\hat{H}$, $\{\Phi\}$. We may go from Φ to a using the basis change matrix $U_{\Phi\to a}(t) \equiv U$, $\boldsymbol{\Psi}_a = U_{\Phi\to a}\boldsymbol{\Psi}_\Phi$. Differentiating this equation,

$$\frac{d\boldsymbol{\Psi}_a}{dt} = \frac{dU}{dt}\boldsymbol{\Psi}_\Phi + U\frac{d\boldsymbol{\Psi}_\Phi}{dt}, \tag{3.13}$$

and substituting in 3.12, using also $H_a = UH_\Phi U^\dagger$ and

$$U^\dagger U = I \Rightarrow \frac{dU}{dt} = -U\frac{dU^\dagger}{dt}U, \tag{3.14}$$

we obtain

$$\frac{d\boldsymbol{\Psi}_\Phi}{dt} = (-iH_\Phi(t) + D)\boldsymbol{\Psi}_\Phi, \tag{3.15}$$

where we defined

$$D_{ij} \equiv \left(\frac{dU^\dagger}{dt}U\right)_{ij} = \left(\frac{d\,\langle E_i|}{dt}\right)|E_j\rangle\,, \tag{3.16}$$

with $|E_i(t)\rangle$ being the eigenstate i of $\hat{H}(t)$. Since the basis is orthonormal, $\langle E_i | E_j \rangle = \delta_{ij}$,

$$\frac{d\,\langle E_i|}{dt}\,|E_j\rangle = -\,\langle E_i|\,\frac{d\,|E_j\rangle}{dt} = -\left(\frac{d\,\langle E_j|}{dt}\,|E_i\rangle\right)^*, \tag{3.17}$$

so D is an anti-hermitian matrix just like $-iH_\Phi$, and it is independent of the basis a. H_Φ is the diagonalized Hamiltonian and accounts for the evolution due to the (time dependent) energies. If D were zero, the time dependence would be of the usual form $\exp(-i\int_0^t E(t')dt')$. D accounts for the fact that the eigenspace basis is changing with time. If we were working on a real and not complex space, the change of the basis over time could be expressed with a rotation matrix and D would be a real, anti-symmetric matrix. Let us say that D is a diagonal matrix. Then the solution of 3.15 is

$$\Psi_i(t) = \exp\left[-i\int_0^t \left(E_i(t') + i\left\langle E_i'|E_i\right\rangle(t')\right)dt'\right]\Psi_i(0), \tag{3.18}$$

where we wrote $\langle E_i'| \equiv d\langle E_i|/dt$. The diagonal elements of D, which are imaginary if the states norm does not change over time, give rise to the second integral which is known as the Berry phase.[28] The Berry phase depends on our choice of basis. For example, we may remove the diagonal elements by a basis transformation. If $\langle E_i'|E_i\rangle = if_i(t)$, with $f_i(t)$ a real function, the transformation

$$|E_i(t)\rangle \to \exp(i\int_0^t f_i(t')dt')\,|E_i(t)\rangle \tag{3.19}$$

will make $D_{ii} = 0$. What is invariant is the closed loop Berry phase (we could call it a Berry flux, analogous to the vector potential), meaning the following: let us say we choose the basis where $D_{ii} = 0$, effectively absorbing the Berry phase into the states. If, in our time evolution, at $t = t_2$ we return to a basis of states that we have already been at, at $t = t_1$, there may be a relative phase between each pair of states, $\langle E_i(t_1)|E_i(t_2)\rangle = e^{i\theta_{ij}}$. The phases are independent of our choice of basis, only depending on the path of Hamiltonian parameters we took from t_1 to t_2. The path of *parameter* we chose is $\Phi = wt$ and we might return periodically to the same eigenspace. Still, the closed loop Berry phase, even if it is not zero, should not be important for this work.

The off-diagonal elements of D can be calculated the following way: since $|E\rangle$ are eigenstates of $\hat{H}$, $\langle E_i|\hat{H} = E_i\langle E_i|$. Differentiating, we get

$$\langle E_i'|\hat{H} + \langle E_i|\hat{H}' = E_i'\langle E_i| + E_i\langle E_i'|, \tag{3.20}$$

where $\hat{H}' = d\hat{H}/dt$. The projection in $|E_j\rangle$ gives us,

$$\langle E_i|\hat{H}'|E_j\rangle = E_i'\delta_{ij} + (E_i - E_j)\langle E_i'|E_j\rangle. \tag{3.21}$$

If $E_i \neq E_j$, we may calculate D_{ij} from $\langle E_i|\hat{H}'|E_j\rangle/(E_i - E_j)$. If the energies cross at a point, we will have a $0/0$ indetermination, but there will be continuity and differentiability in all functions, so we may take the limit $\Delta E \to 0$. If both states belong to the same degenerate subspace, like the localized states, we will have to calculate $\langle E_i'|E_j\rangle$ directly, which was expected since the rotation inside the subspace will depend on our choice of basis for that subspace.

3.2.1 Rotational symmetry in the eigenstate transitions

Consider two eigenstates $|\Psi\rangle$ and $|\Gamma\rangle$ of energies $E_\Psi \neq E_\Gamma$. The element of transition D_{ij} will be proportional to $\langle\Psi|\,\hat{H}'\,|\Gamma\rangle$, where the time derivative of $\hat{H}$ (Eq. 2.7) is

$$\begin{aligned}\hat{H}' = &\sum_{x=-L,2}^{L}\sum_{y=-L}^{L-1}\left(-i\int_{x,y}^{x,y+1}\boldsymbol{E}\cdot d\boldsymbol{r}\right)\exp\left(i\int_{x,y}^{x,y+1}\boldsymbol{A}\cdot d\boldsymbol{r}\right)|x,y+1\rangle\langle x,y| + H.c.\\ &+\sum_{y=-L,2}^{L}\sum_{x=-L}^{L-1}\left(-i\int_{x,y}^{x+1,y}\boldsymbol{E}\cdot d\boldsymbol{r}\right)\exp\left(i\int_{x,y}^{x+1,y}\boldsymbol{A}\cdot d\boldsymbol{r}\right)|x+1,y\rangle\langle x,y| + H.c.\ .\end{aligned} \tag{3.22}$$

We performed the derivative only on the matrix elements since the lattice states are time independent. Notice that we can change the vector potential through a time dependent gauge transformation of the lattice states, but if we did so before performing the derivative, we would have to differentiate the lattice states too. Simply put, the electric field integral term is not altered through a gauge transformation. From Eq.3.22 we can interpret that the electric field is the sole responsible for transitions between levels of different energies. The matrix element of $\hat{H}'$ is given by

$$\begin{aligned}i\,\langle\Psi|\,\hat{H}'\,|\Gamma\rangle = &\sum_{x=-L,2}^{L}\sum_{y=-L}^{L-1}\int_{x,y}^{x,y+1}\boldsymbol{E}\cdot d\boldsymbol{r}\exp\left(i\int_{x,y}^{x,y+1}\boldsymbol{A}\cdot d\boldsymbol{r}\right)\Psi^*_{x,y+1}\Gamma_{x,y} + (y\leftrightarrow y+1)\\ &+\sum_{y=-L,2}^{L}\sum_{x=-L}^{L-1}\int_{x,y}^{x+1,y}\boldsymbol{E}\cdot d\boldsymbol{r}\exp\left(i\int_{x,y}^{x+1,y}\boldsymbol{A}\cdot d\boldsymbol{r}\right)\Psi^*_{x+1,y}\Gamma_{x,y} + (x\leftrightarrow x+1).\end{aligned} \tag{3.23}$$

After performing the derivative, the gauge freedom becomes very useful. It will be convenient to use the gauge with the most symmetry possible, $\boldsymbol{A}\propto(-y,x)$. In this gauge, the states Ψ and Γ will be invariant under the C_4 rotations, with invariance phases u_4 (section 2.6). Let us express their invariance as $\Psi_{-y,x}=i^a\Psi_{x,y}$, $\Gamma_{-y,x}=i^b\Gamma_{x,y}$, with $a,b=0,\ldots,3$. From this we get $\Psi^*_{x+1,y}\Gamma_{x,y}=i^{a-b}\Psi^*_{-y,x+1}\Gamma_{-y,x}$. The gauge is also invariant under rotations, so we have $\int_{x,y}^{x+1,y}\boldsymbol{A}\cdot d\boldsymbol{r}=\int_{-y,x}^{-y,x+1}\boldsymbol{A}\cdot d\boldsymbol{r}$. Using this in the second term we get

$$\begin{aligned}i\,\langle\Psi|\,\hat{H}'\,|\Gamma\rangle = &\sum_{x=-L,2}^{L}\sum_{y=-L}^{L-1}\int_{x,y}^{x,y+1}\boldsymbol{E}\cdot d\boldsymbol{r}\exp\left(i\int_{x,y}^{x,y+1}\boldsymbol{A}\cdot d\boldsymbol{r}\right)\Psi^*_{x,y+1}\Gamma_{x,y} + (y\leftrightarrow y+1)\\ &+\sum_{y=-L,2}^{L}\sum_{x=-L}^{L-1}i^{a-b}\int_{x,y}^{x+1,y}\boldsymbol{E}\cdot d\boldsymbol{r}\exp\left(i\int_{-y,x}^{-y,x+1}\boldsymbol{A}\cdot d\boldsymbol{r}\right)\Psi^*_{-y,x+1}\Gamma_{-y,x} + (x\leftrightarrow x+1).\end{aligned} \tag{3.24}$$

Changing the summation indices in the lower sums by $x \to y, y \to -x$, both terms will become equal except on the $\boldsymbol{E}$ integral:

$$\begin{aligned} i \langle \Psi | \hat{H}' | \Gamma \rangle = \sum_{x=-L,2}^{L} \sum_{y=-L}^{L-1} \left(\int_{x,y}^{x,y+1} \boldsymbol{E} \cdot d\boldsymbol{r} + i^{a-b} \int_{y,-x}^{y+1,-x} \boldsymbol{E} \cdot d\boldsymbol{r} \right) \\ \exp\left(i \int_{x,y}^{x,y+1} \boldsymbol{A} \cdot d\boldsymbol{r} \right) \Psi^*_{x,y+1} \Gamma_{x,y} + (y \leftrightarrow y+1). \end{aligned} \tag{3.25}$$

Let us divide the summation in to two intervals of y, and write down the downwards jump terms $\Psi^*_{x,y}\Gamma_{x,y+1}$ instead of the upwards in the second term,

$$\begin{aligned} i \langle \Psi | \hat{H}' | \Gamma \rangle = \sum_{x=-L,2}^{L} \sum_{y=0}^{L-1} \left(\int_{x,y}^{x,y+1} \boldsymbol{E} \cdot d\boldsymbol{r} + i^{a-b} \int_{y,-x}^{y+1,-x} \boldsymbol{E} \cdot d\boldsymbol{r} \right) \\ \exp\left(i \int_{x,y}^{x,y+1} \boldsymbol{A} \cdot d\boldsymbol{r} \right) \Psi^*_{x,y+1} \Gamma_{x,y} + (y \leftrightarrow y+1) \\ + \sum_{x=-L,2}^{L} \sum_{y=-L}^{-1} \left(\int_{x,y+1}^{x,y} \boldsymbol{E} \cdot d\boldsymbol{r} + i^{a-b} \int_{y+1,-x}^{y,-x} \boldsymbol{E} \cdot d\boldsymbol{r} \right) \\ \exp\left(i \int_{x,y+1}^{x,y} \boldsymbol{A} \cdot d\boldsymbol{r} \right) \Psi^*_{x,y} \Gamma_{x,y+1} + (y \leftrightarrow y+1). \end{aligned} \tag{3.26}$$

Using the change of indices $y \to -(y+1), x \to -x$ in the second term,

$$\begin{aligned} i \langle \Psi | \hat{H}' | \Gamma \rangle = \sum_{x=-L,2}^{L} \sum_{y=0}^{L-1} \left(\int_{x,y}^{x,y+1} \boldsymbol{E} \cdot d\boldsymbol{r} + i^{a-b} \int_{y,-x}^{y+1,-x} \boldsymbol{E} \cdot d\boldsymbol{r} \right) \\ \exp\left(i \int_{x,y}^{x,y+1} \boldsymbol{A} \cdot d\boldsymbol{r} \right) \Psi^*_{x,y+1} \Gamma_{x,y} + (y \leftrightarrow y+1) \\ + \sum_{x=-L,2}^{L} \sum_{y=0}^{L-1} \left(\int_{-x,-y}^{-x,-(y+1)} \boldsymbol{E} \cdot d\boldsymbol{r} + i^{a-b} \int_{-y,x}^{-(y+1),x} \boldsymbol{E} \cdot d\boldsymbol{r} \right) \\ \exp\left(i \int_{-x,-y}^{-x,-(y+1)} \boldsymbol{A} \cdot d\boldsymbol{r} \right) \Psi^*_{-x,-(y+1)} \Gamma_{-x,-y} + (y \leftrightarrow y+1). \end{aligned} \tag{3.27}$$

Again by the rotational invariance we have $\Psi^*_{-x,-(y+1)}\Gamma_{-x,-y} = i^{2(a-b)}\Psi^*_{x,y+1}\Gamma_{x,y}$, the $\boldsymbol{A}$ integrals are equal and the terms will merge, so $i \langle \Psi | \hat{H}' | \Gamma \rangle$ is

$$\begin{aligned} \sum_{x=-L,2}^{L} \sum_{y=0}^{L-1} \left(\int_{x,y}^{x,y+1} \boldsymbol{E} \cdot d\boldsymbol{r} + i^{a-b} \int_{y,-x}^{y+1,-x} \boldsymbol{E} \cdot d\boldsymbol{r} + i^{2(a-b)} \int_{-x,-y}^{-x,-(y+1)} \boldsymbol{E} \cdot d\boldsymbol{r} \right. \\ \left. + i^{3(a-b)} \int_{-y,x}^{-(y+1),x} \boldsymbol{E} \cdot d\boldsymbol{r} \right) \exp\left(i \int_{x,y}^{x,y+1} \boldsymbol{A} \cdot d\boldsymbol{r} \right) \Psi^*_{x,y+1} \Gamma_{x,y} + (y \leftrightarrow y+1). \end{aligned} \tag{3.28}$$

The D matrix element between states Ψ, Γ with C_4 rotation constants i^a, i^b, respectively can then be written as

$$\langle \Psi' | \Gamma \rangle = \frac{1}{i(E_\Psi - E_\Gamma)} \sum_{x=-L,2}^{L} \sum_{y=0}^{L-1} P_4(\boldsymbol{E}) \exp\left(i \int_{x,y}^{x,y+1} \boldsymbol{A} \cdot d\boldsymbol{r} \right) \Psi^*_{x,y+1} \Gamma_{x,y} + (y \leftrightarrow y+1), \tag{3.29}$$

where we defined

$$P_4(\boldsymbol{E}) = \sum_{n=0}^{3} i^{n(a-b)} \int_{x,y}^{x,y+1} (\hat{R}^n_{\frac{\pi}{2}} \boldsymbol{E}) \cdot d\boldsymbol{r}, \tag{3.30}$$

where the rotation operator, since it is being applied to a vector field and not a scalar field like the wave function, rotates both the electric field vectors and the points of application. It is easy to see now that the transition terms of an arbitrary lattice with C_N symmetry can be written as a sum over $1/N$ of the total number of connections, each term of the sum with a dependence on the electric field of the kind of

$$P_N(\boldsymbol{E}) = \sum_{n=0}^{N-1} e^{i\frac{2\pi}{N} n(a-b)} \int_{x,y}^{x,y+1} (\hat{R}^n_{\frac{2\pi}{N}} \boldsymbol{E}) \cdot d\boldsymbol{r}, \tag{3.31}$$

with $a, b = 0, \ldots, N-1$. For certain lattices the path of integration may have to be different. Let us see what we obtain for the circular and the uniform electric fields. For $\boldsymbol{E} = \mathcal{E}(-y, x)$, $\hat{R}^n_{\frac{2\pi}{N}} \boldsymbol{E} = \boldsymbol{E}$ and $\int_{x,y}^{x,y+1} \boldsymbol{E} \cdot d\boldsymbol{r} = \mathcal{E} x$, so we have

$$P_N(\mathcal{E}(-y, x)) = \mathcal{E} x \sum_{n=0}^{N-1} e^{i\frac{2\pi}{N} n(a-b)} = \mathcal{E} x N \delta_{a,b}. \tag{3.32}$$

This means there are no transitions between states of different rotation phases, so any state that is u_4 invariant initially will only gain components over time in states with the same u_4, maintaining its original invariance phase. For $\boldsymbol{E} = \mathcal{E}(\cos\alpha, \sin\alpha)$, we have $\hat{R}^n_{\frac{2\pi}{N}} \boldsymbol{E} = \mathcal{E}(\cos(\alpha + \frac{2\pi}{N} n), \sin(\alpha + \frac{2\pi}{N} n))$ and $\int_{x,y}^{x,y+1} \boldsymbol{E} \cdot d\boldsymbol{r} = \mathcal{E} \sin(\alpha + \frac{2\pi}{N} n)$, so we get

$$\begin{aligned} P_N(\mathcal{E}(\cos\alpha, \sin\alpha)) &= \frac{\mathcal{E}}{2i} \sum_{n=0}^{N-1} e^{i\frac{2\pi}{N} n(a-b)} \left(e^{i(\alpha + \frac{2\pi}{N} n)} - e^{-i(\alpha + \frac{2\pi}{N} n)} \right) \\ &= \frac{\mathcal{E}}{2i} \sum_{n=0}^{N-1} e^{i\alpha} e^{i\frac{2\pi}{N} n(a-b+1)} - e^{-i\alpha} e^{i\frac{2\pi}{N} n(a-b-1)} \\ &= \frac{\mathcal{E} N}{2i} \left(e^{i\alpha} \delta_{a+1,b} - e^{-i\alpha} \delta_{a,b+1} \right). \end{aligned} \tag{3.33}$$

Now we have jumps between neighbouring rotation phases, which result in indirect jumps between all rotation phases, so states may eventually gain components in all the eigenstates. Our electric field of choice has both a uniform component and a circular component (Eq.3.9). We have

$$P_4(-\frac{\partial \boldsymbol{A}}{\partial t}) = \frac{\omega}{2} x \delta_{a,b} + \frac{\omega r_0}{4i} \left(e^{i\alpha} \delta_{a+1,b} - e^{-i\alpha} \delta_{a,b+1} \right), \tag{3.34}$$

where $r_0 = \sqrt{x_0^2 + y_0^2}$ and $\tan\alpha = -x_0/y_0$. We know directly that the transitions elements with $P_4 = 0$ are zero, but some elements might be zero even if the electric field permits the transition due to other symmetries of the system. This is the case of the secondary diagonal elements, which are zero due to the $\pm E$ symmetry.

3.2.2 Positive-negative energy symmetry

As we saw already in section 2.5, the itinerant states of the Lieb lattice come in pairs. Let us see how this affects the matrix D. Consider the states from equation 2.12. The main and secondary diagonal terms are

$$\begin{aligned} \langle E'_+|E_+\rangle = \langle E'_-|E_-\rangle = 1/2(\langle A'|A\rangle + \langle BC'|BC\rangle), \\ \langle E'_+|E_-\rangle = \langle E'_-|E_+\rangle = 1/2(\langle A'|A\rangle - \langle BC'|BC\rangle), \end{aligned} \tag{3.35}$$

where we used $\langle A'|BC\rangle = \langle BC'|A\rangle = 0$. Note that all the equalities above are true only in our particular choice of states $|E_\pm\rangle$. We could multiply each state by different time dependent phases and the equalities would no longer hold true. Now, while a basis transformation adds or subtracts a term in the main diagonal terms, the off-diagonal terms will be multiplied by a phase, not changing the absolute value. In this choice of states $\langle E'_+|E_-\rangle$ is imaginary since $\langle A|A\rangle = \langle BC|BC\rangle = 1$. Let us calculate $\langle E_+|\,\hat{H}'\,|E_-\rangle$. Both states have the same u_4, so, from the previous section, we have

$$\langle E_+|\,\hat{H}'\,|E_-\rangle = \frac{\omega}{2i}\sum_{x=-L,2}^{L}\sum_{y=0}^{L-1} x \exp\left(i\int_{x,y}^{x,y+1}\boldsymbol{A}\cdot d\boldsymbol{r}\right)(E_+)^*_{x,y+1}(E_-)_{x,y} + (y \leftrightarrow y+1). \tag{3.36}$$

Both states are related by the BC to minus BC transformation $\hat{T}_{BC} = (-1)^{x+y}$, so that $(E_-)_{x,y} = (-1)^{x+y}(E_+)_{x,y}$. Using this and writing explicitly the conjugate jump term $(y \leftrightarrow y+1)$, we have

$$\begin{aligned} \langle E_+|\,\hat{H}'\,|E_-\rangle = \frac{\omega}{2i}\sum_{x=-L,2}^{L} x\sum_{y=0}^{L-1}(-1)^{x+y}\exp\left(i\int_{x,y}^{x,y+1}\boldsymbol{A}\cdot d\boldsymbol{r}\right)(E_+)^*_{x,y+1}(E_+)_{x,y} \\ -(-1)^{x+y}\exp\left(-i\int_{x,y}^{x,y+1}\boldsymbol{A}\cdot d\boldsymbol{r}\right)(E_+)^*_{x,y}(E_+)_{x,y+1}, \end{aligned} \tag{3.37}$$

$$\langle E_+|\,\hat{H}'\,|E_-\rangle = \omega\sum_{x=-L,2}^{L} x\sum_{y=0}^{L-1}(-1)^{x+y}\ \mathrm{Im}\left(\exp\left(i\int_{x,y}^{x,y+1}\boldsymbol{A}\cdot d\boldsymbol{r}\right)(E_+)^*_{x,y+1}(E_+)_{x,y}\right), \tag{3.38}$$

so we conclude that $\langle E'_+|E_-\rangle$ is real, but, as we saw before, it is also imaginary, so it must be zero. Note that for other electric fields this result may no longer hold: if $P_4(\boldsymbol{E})$ depended on y, the direction of the jumps, we could no longer conclude that $\langle E'_+|E_-\rangle = 0$. We have then

$$\begin{aligned} \langle E'_+|E_+\rangle = \langle E'_-|E_-\rangle = \langle A'|A\rangle = \langle B'|B\rangle\,, \\ \langle E'_+|E_-\rangle = \langle E'_-|E_+\rangle = 0, \end{aligned} \tag{3.39}$$

and, as we have already seen, we may put the diagonal elements to zero. Other elements we are interested in are the ones involving a localized state $|L\rangle$. With our choice of states $|E_\pm\rangle$, we have the relation

$$\langle E'_+|L\rangle = -\langle E'_-|L\rangle = \langle BC'|L\rangle /\sqrt{2}, \tag{3.40}$$

since localized states only have a BC component.

3.3 Localized basis freedom

There is a basis of the localized subspace where all the states are C_4 invariant, so that all the terms $\langle E'_+|L_i\rangle$ follow the already known behaviour in terms of the electric field. It is possible, through a basis transformation of the localized subspace, to make it so only one of the localized states rotates with an itinerant state, $\langle E'_+|L_i\rangle = f(t)\delta_{ij}$, for some j. The basis where that is true can be built from a generic basis like this: consider a sequence of localized states $|L_i\rangle$ from 1 to N_l and a state $|E\rangle$. The basis transformation

$$\begin{aligned} |L_1\rangle &\leftarrow \langle E'|L_1\rangle^* |L_1\rangle + \langle E'|L_2\rangle^* |L_2\rangle , \\ |L_2\rangle &\leftarrow \langle E'|L_2\rangle |L_1\rangle - \langle E'|L_1\rangle |L_2\rangle , \end{aligned} \tag{3.41}$$

results in $\langle L_1|L_2\rangle = \langle E'|L_2\rangle = 0$, so that the rotation from both states was absorbed into $|L_1\rangle$. Subsequent transformations for all pairs $(1, i)$, $i = 2, \ldots, N_l$, will absorb the full rotation of the localized subspace with $|E\rangle$ into a single localized state, the new $|L_1\rangle$. It is easy to see that state will be

$$|L_1\rangle \leftarrow \frac{\sum_{i=1}^{N_l} \langle E'|L_i\rangle^* |L_i\rangle}{\sqrt{\sum_{i=1}^{N_l} |\langle E'|L_i\rangle|^2}}. \tag{3.42}$$

However, this transformation has altered the diagonal elements so that $\langle L'_1|L_1\rangle \neq 0$. From Eq.3.19 we know how to remove it, giving us

$$|L_1\rangle \leftarrow \exp\left[i\mathrm{Im}\left(\int \frac{\sum_{i=1}^{N_l} (\langle E'|L_i\rangle)' \langle E'|L_i\rangle^*}{\sum_{i=1}^{N_l} |\langle E'|L_i\rangle|^2} dt\right)\right] \frac{\sum_{i=1}^{N_l} \langle E'|L_i\rangle^* |L_i\rangle}{\sqrt{\sum_{i=1}^{N_l} |\langle E'|L_i\rangle|^2}}. \tag{3.43}$$

Just as a side note, we can write this in a more compact form as

$$|L_1\rangle \leftarrow C \exp\left[\int \frac{\sum_{i=1}^{N_l} (\langle E'|L_i\rangle)' \langle E'|L_i\rangle^*}{\sum_{i=1}^{N_l} |\langle E'|L_i\rangle|^2} dt\right] \sum_{i=1}^{N_l} \langle E'|L_i\rangle^* |L_i\rangle , \tag{3.44}$$

where the real part of the integral guarantees constant normalization and the imaginary part removes the Berry phase, and C is some normalization constant. The full rotation is, from Eq.3.43,

$$\langle E'|L_1\rangle \leftarrow e^{i\theta_1(t)} \sqrt{\sum_{i=1}^{N_l} |\langle E'|L_i\rangle|^2}, \tag{3.45}$$

where θ_1 is the imaginary part of the integral. The same transformation could be used so that a localized state rotates only with another localized state. For example, after transforming $|L_1\rangle$, we can apply the transformation

$$|L_2\rangle \leftarrow e^{i\theta_2(t)} \frac{\sum_{i=2}^{N_l} \langle L_1'|L_i\rangle^* |L_i\rangle}{\sqrt{\sum_{i=2}^{N_l} |\langle E'|L_i\rangle|^2}}. \tag{3.46}$$

The state $|L_2\rangle$ will now be the one that rotates alone with $|L_1\rangle$. Subsequent equivalent transformations allow us to off-diagonalize D in the subspace $\{|E\rangle, |L_i\rangle\}$.

3.3.1 Two by two lattice

We can obtain several analytical results for the 2×2 Lieb lattice (Fig. 2.1). It has three localized states, and the matrix D in the subspace of localized states plus the pair of S states, $\{|S_+\rangle, |L_i\rangle, |S_-\rangle\}$, can be written as

$$D = \begin{pmatrix} 0 & f & 0 & 0 & 0 \\ -f^* & 0 & a & 0 & f^* \\ 0 & -a^* & 0 & b & 0 \\ 0 & 0 & -b^* & 0 & 0 \\ 0 & -f & 0 & 0 & 0 \end{pmatrix}, \tag{3.47}$$

for some basis of the localized subspace, where we used the localized basis freedom and the $\pm E$ symmetry properties. We chose this subspace because the rotation of localized states with S states is the most important in a slow time evolution. In a 2×2 lattice, at $\Phi = 0$ we have four localized states, which we may combine to make one state for each possible value of u_4, $1, -1, i, -i$. The state that is lost to the S states is the one with symmetry $u_4 = 1$ (remember that in a lattice of size $L \times L$, the S states have $u_4 = (-1)^L$). Given our electric field, the S states will only rotate with the $\pm i$ states through the uniform electric field. There are two two-plaquette localized states that are known analytically, one in each diagonal of the lattice. For the vector potential in Eq.3.9, the states amplitudes (here represented in the lattice sites basis and in the shape of the 2×2 Lieb lattice) are given by

$$\sqrt{8}\,|L_+\rangle = \begin{pmatrix} 0 & 0 & 0 & e^{i\phi(2-2x_0+y_0)} & 0 \\ 0 & & -e^{i\phi(4-x_0)} & & -e^{i\phi(-2-x_0+2y_0)} \\ 0 & -e^{i\phi(-4-y_0)} & 0 & e^{i\phi(-4+y_0)} & 0 \\ e^{i\phi(-2+x_0-2y_0)} & & e^{i\phi(4+x_0)} & & 0 \\ 0 & -e^{i\phi(2+2x_0-y_0)} & 0 & 0 & 0 \end{pmatrix}, \tag{3.48}$$

$$\sqrt{8}\,|L_-\rangle = \begin{pmatrix} 0 & -e^{i\phi(-2-2x_0-y_0)} & 0 & 0 & 0 \\ e^{i\phi(2-x_0-2y_0)} & & e^{i\phi(-4-x_0)} & & 0 \\ 0 & -e^{i\phi(4-y_0)} & 0 & e^{i\phi(4+y_0)} & 0 \\ 0 & & -e^{i\phi(-4+x_0)} & & -e^{i\phi(2+x_0+2y_0)} \\ 0 & 0 & 0 & e^{i\phi(-2+2x_0+y_0)} & 0 \end{pmatrix}, \tag{3.49}$$

with $\phi = \Phi/8$. They are not orthogonal for a general uniform electric field except at $\Phi = 0$. Close to $\Phi = 0$, the states $|L_{\pm i}\rangle = (|L_+\rangle \pm i\,|L_-\rangle)/\sqrt{2}$ will be approximately orthogonal, and $|L_{\pm i}\rangle$ have $u_4 = \pm i$ with no uniform electric field. The remaining state of the basis will have $u_4 = -1$ and will not rotate with $|S_\pm\rangle$. In the 2×2 lattice $|S_+\rangle$ only has BC component at the edge states and they alternate between ± 1 from BC site to BC site, so we can calculate explicitly $\langle L'_\pm|S_+\rangle$ at $\Phi = 0$, calculating the derivatives of the states above. We obtain $\langle L'_\pm(0)|S_+(0)\rangle = -\langle S'_+(0)|L_\pm(0)\rangle^* = C(\pm y_0 - x_0)$, with C a constant. We can combine both states and condense the rotation into one state, which we shall call $|L_S\rangle$:

$$|L_S\rangle = -\frac{\langle L'_+|S_+\rangle\,|L_+\rangle + \langle L'_-|S_+\rangle\,|L_-\rangle}{\sqrt{|\langle L'_+|S_+\rangle|^2 + |\langle L'_-|S_+\rangle|^2}} = \frac{(x_0 - y_0)\,|L_+\rangle + (x_0 + y_0)\,|L_-\rangle}{r_0\sqrt{2}}, \tag{3.50}$$

with $r_0 = \sqrt{x_0^2 + y_0^2}$. Substituting $(-y_0, x_0) = r_0(\cos\alpha, \sin\alpha)$, where $(-y_0, x_0)$ is proportional to the uniform electric field, we obtain

$$\begin{aligned} |L_S\rangle &= \left[(\cos\alpha + \sin\alpha)\,|L_+\rangle + (\sin\alpha - \cos\alpha)\,|L_-\rangle\right]/\sqrt{2} \\ &= \cos(\alpha - \pi/4)\,|L_+\rangle - \cos(\alpha + \pi/4)\,|L_-\rangle\,. \end{aligned} \tag{3.51}$$

This means whenever the electric field is aligned with one of the diagonals, $\alpha = \pm\pi/4$, the localized states that rotates alone with $|S\rangle$ is the two-plaquette localized state in that diagonal, at least for $\Phi \approx 0$, and when we rotate the electric field, so will the state rotate to keep pointing in the direction of the field. A similar behaviour could be expected for larger lattices.

There is one more property of the 2×2 lattice which will be important, and is that there is a basis of states where the matrix D is anti-symmetric. In the form of Eq. 3.47, the off-diagonal elements may be complex, but they will be real functions multiplied by a constant phase, for example, $f(t) = r(t)e^{i\theta}$, with $r(t)$ a real function. The phases of each off-diagonal term can be absorbed into the states so that D becomes anti-symmetric. This was found by the numerical calculation of D and does not happen for larger lattices, and also makes the time evolution in the 2×2 lattice especially simpler.

3.4 S to localized state transition

In the 2×2 lattice the dependence on $\boldsymbol{E}$ of $\langle S'_+|L_S\rangle$ is simple: two localized states with $u_4 = \pm i$ couple to $|S_\pm\rangle$ through the uniform electric field $\boldsymbol{E}_0$, so from Eq.3.45 we get

$$\begin{aligned}\langle S'_+|L_S\rangle &= e^{i\theta(t)}\sqrt{|\langle S'_+|L_{-i}\rangle|^2 + |\langle S'_+|L_i\rangle|^2} \\ &= |\boldsymbol{E}_0|e^{i\theta(t)}\sqrt{|f_{-i}|^2 + |f_i|^2},\end{aligned} \tag{3.52}$$

for some functions $f_{\pm i}$ that do not depend on $\boldsymbol{E}$. For all values of flux the transition term is proportional to the uniform electric field. For larger lattices we can not conclude the same, but we can separate the summation in Eq.3.45 in two, one for states with neighbour C_4 invariances of S_+, $u_4 = \pm i$, and another with equal C_4 invariance, $u_4 = (-1)^L$,

$$\langle S'_+|L_S\rangle = e^{i\theta(t)}\sqrt{|\boldsymbol{E}_0|^2\sum_{n,u_4=\pm i}|f_n|^2 + \sum_{m,u_4=(-1)^L}|\langle S'_+|L_m\rangle|^2}. \tag{3.53}$$

We can, however, conclude something about the behaviour with electric field at $\Phi = 0$ using the reflection symmetries. Consider the product

$$\langle BC(\Phi)|L_m(0)\rangle = \langle S_+(\Phi)|L_m(0)\rangle = \sum_{n=1}^{\infty}\frac{d^n\langle S_+(0)|}{d\Phi^n}|L_m(0)\rangle\frac{\Phi^n}{n!}. \tag{3.54}$$

Remember from Section 2.6 that the localized states and the BC state of the S states have a relation between σ and C_4 invariance phases, $u_\sigma = -u_4$. For $u_4 = (-1)^L$ we have

$$\hat{R}_\sigma|BC(\Phi)\rangle = (-1)^{L+1}|BC(-\Phi)\rangle, \tag{3.55}$$

$$\hat{R}_\sigma|L_m(0)\rangle = (-1)^{L+1}|L_m(0)\rangle. \tag{3.56}$$

Applying the rotation to Eq.3.54,

$$\langle BC(\Phi)|\hat{R}_\sigma\hat{R}_\sigma|L_m(0)\rangle = \langle BC(-\Phi)|L_m(0)\rangle, \tag{3.57}$$

we conclude 3.54 is an even function, so odd terms of its expansion are zero, the first term being $\langle S'_+(0)|L_v(0)\rangle = 0$. Substituting in Eq. 3.53 for zero or equivalent flux $\Phi = 2\pi n$, we find that the transition term is proportional to the uniform electric field,

$$\langle S'_+|L_S\rangle(\Phi = 2\pi n) \propto |\boldsymbol{E}_0| = \omega/8\sqrt{x_0^2 + y_0^2}. \tag{3.58}$$

We shall see the consequence of this together with the numerical results.

Chapter 4

Numerical time evolution of localized states

In this chapter we present the results of numerical time evolutions of two-plaquette localized states for $L = 2$ and $L = 6$, for different uniform electric field components, starting positions and ω. We then discuss the step pattern that appears in some simulations with finite electric field. Before all that, we show the algorithm used in the simulations.

4.1 Numerical algorithm

Consider a state $\mathbf{\Psi}_a(t)$, in a time independent basis $\{a\}$, and the time evolution equation $id\mathbf{\Psi}_a/dt = H_a(t)\mathbf{\Psi}_a$. The relation between two points distanced by dt is

$$\mathbf{\Psi}_a(t + dt) = \exp(-iH_a(t)dt)\mathbf{\Psi}_a(t). \tag{4.1}$$

Consider again the matrix of basis change from the eigenspace of $\hat{H}$, $U_{\Phi\to a}(t)$, so that

$$\mathbf{\Psi}_a(t + dt) = U(t)\exp(-iH_\Phi(t)dt)U^\dagger(t)\mathbf{\Psi}_a(t). \tag{4.2}$$

This equation allows us to calculate the evolution of $\mathbf{\Psi}_a$ iteratively for some finite dt. The time step is related to the flux step: $\Delta t = \Delta\Phi/\omega$. The flux is more useful in identifying where in the evolution we are, and since we chose a linear evolution in the flux, it is easy to transform the equations to use the flux instead of time. We are interested in the decomposition of $|\Psi\rangle$ in the eigenspace, so we should calculate $U^\dagger(\Phi)\mathbf{\Psi}_a(\Phi)$ too. The basis $\{a\}$ will be the lattice sites basis. Diagonalizing numerically $H_a(\Phi)$ (Eq. 2.7) using the vector potential from Eq. 3.9 we obtain the diagonalized Hamiltonian $H_\Phi(\Phi)$ and the eigenstates $U(\Phi)$. The following algorithm shows the time evolution in pseudo-code. It calculates $\mathbf{\Psi}_\Phi$ over time and was implemented in MATLAB.[26]

Data: $\Phi_0, \Delta\Phi, \Phi_l$, $\mathbf{\Psi}_a(\Phi_0)$, x_0, y_0, L, ω
for $\Phi \leftarrow \Phi_0, \Phi_0 + \Delta\Phi, \ldots, \Phi_l$ **do**
  $H_a \leftarrow$ Eq.2.7;
  $\{H_\Phi, U\} \leftarrow$ Diagonalize(H_a);
  $\mathbf{\Psi}_\Phi(\Phi) = U^\dagger\mathbf{\Psi}_a(\Phi)$;
  $\mathbf{\Psi}_a(\Phi + \Delta\Phi) = U\exp(-iH_\Phi\Delta\Phi/\omega)\mathbf{\Psi}_\Phi(\Phi)$;
end

4.2 Time evolution simulations

For the simulations in this section we used $\omega = 0.01$ and $\Delta\Phi = 2\pi \times 10^4$, meaning 10^4 points per 2π interval, unless it is stated otherwise.

4.2.1 Two by two lattice

In Fig. 4.1a we have the energy diagram of the 2×2 Lieb lattice. The itinerant states in the four-state sub-bands closest to the flat band are labelled by their rotation phase u_4. In Figs. 4.1b to 4.2b we can see the $|\Psi_n|^2$ components in the eigenstates, where n is the eigenstate index, over time (flux) of a state on an $L = 2$ lattice that started at $\Phi_0 = -\pi$ as $|L_+(\Phi_0)\rangle$ (Eq. 3.48) for five cases of uniform electric field $(-y_0, x_0)$. The components are coloured and labelled by u_4 to match the energy diagram. $(-y_0, x_0)$ is indicated in the caption of each plot.

In Fig. 4.1b, $(-y_0, x_0) = (0, 0)$, all components were plotted except for the localized component. The components on itinerant states of opposite energies $\pm E$ are equal so they are plotted one exactly over the other. The components of the state oscillate with a very high frequency and seem to be periodic. The components on the $\pm i$ states are by far the largest itinerant components. Remember that our initial state is a combination of the $\pm i$ localized states of the 2×2 lattice, and since there is no uniform electric field there are only transitions to states with the same rotational invariance. This prohibits transitions to the S states, to the -1 localized state and to the -1 labelled itinerant states, so those components are zero. However, it does not prohibit the transition to the $\pm i$ states of the other sub-bands, but those components are of the order of 10^{-9} at most. There is a correlation between smaller components and a bigger difference in energy. Notice how the $\pm i$ components increase or decrease when their energy gets closer or further away from zero, the energy of the localized states.

In Fig. 4.1c, $(-y_0, x_0) = (-4.3, 4.3)$, we added a uniform electric field in the $x = -y$ diagonal. Just like in the previous figure, we are not showing the localized component, and components in opposite energy states are equal. An increase in the overall magnitude of the itinerant components is noticeable. We now have non-zero components in all states, but the components in the states of the closest sub-bands still dominate over the rest of itinerant states. The amplitude modulation with the energy difference is also noticeable, but even though the S states are the ones that go closest to the localized states in terms of energy, their component is the smallest between the closest sub-band states. This is explained by the fact that the uniform electric field is perpendicular to the diagonal of the two-plaquette localized state that was used as initial state, $|L_+\rangle$. As we may remember from section 3.3.1, the localized state that rotates alone with the special states at $\Phi = 2\pi n$ is aligned with the uniform electric field, so when the component was supposed to be the biggest, at zero energy, the transition element is also zero, $\langle S'_+|L_+\rangle\,(\Phi = 2\pi n) = 0$ for this electric field, resulting in a much smaller component. It is also noticeable that the frequency of oscillation of the S components is much smaller than the rest when we are close to $\Phi = 2\pi n$. This happens because the oscillation frequency is closely given by the energy difference.

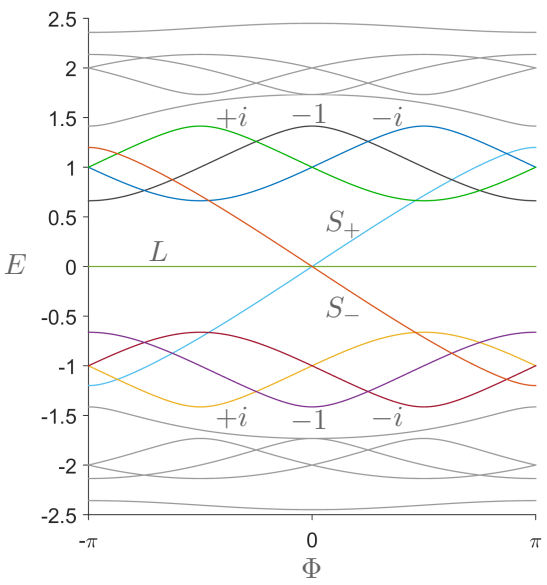

(a)

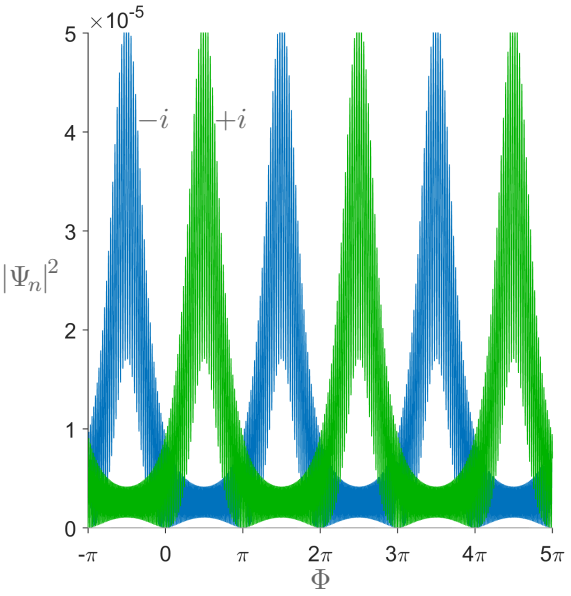

(b) $(-y_0, x_0) = (0, 0)$.

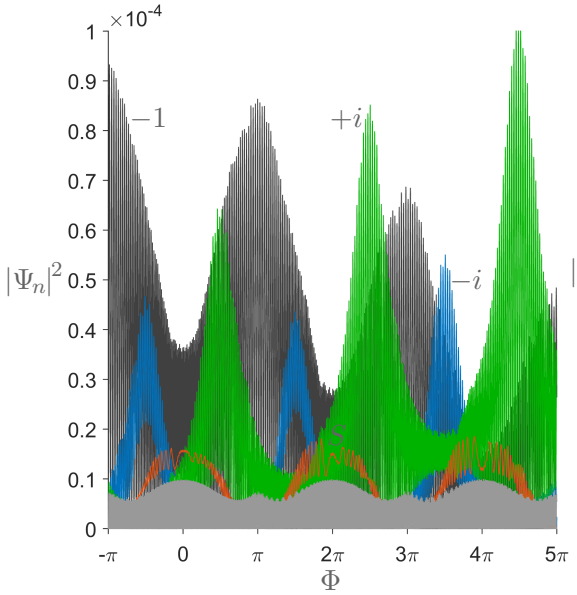

(c) $(-y_0, x_0) = (-4.3, 4.3)$.

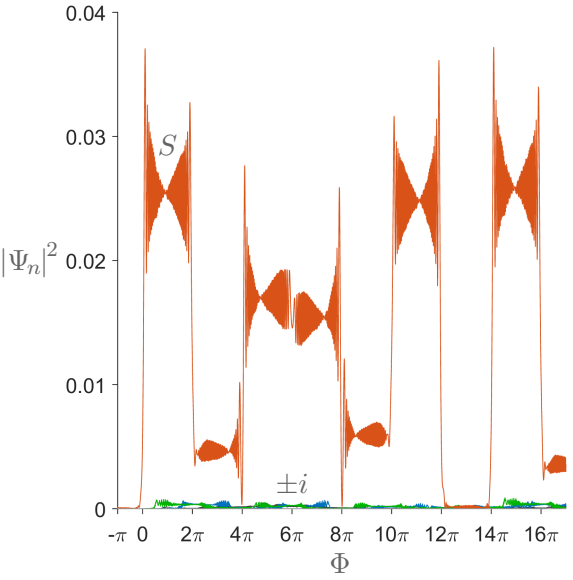

(d) $(-y_0, x_0) = (4.3, 4.3)$.

Figure 4.1: (a) Energy diagram of the 2×2 Lieb lattice. (b,c,d) Components in the eigenstates over time (from simulations) for a localized state that started as $|L_+(-\pi)\rangle$ (Eq. 3.48) on the 2×2 lattice, for three different uniform electric fields.

In Fig. 4.1d, $(-y_0, x_0) = (4.3, 4.3)$, the uniform electric field is now aligned with the initial state. The largest components of single states are of the two S states, which are exactly equal as in the previous figures. The behaviour is different relative to the previous plots. We now have a step-like behaviour of the S state components, which dominate all the others. While previously we seemed to gain or lose components continuously, we now gain or lose a significant portion of the components in the S states at the point the energies cross, $\Phi = 2\pi n$, and we gain or lose it permanently, at least until the next crossing point. Between crossing points we have an oscillation of high frequency around the newly gained component. The frequency decreases close to the crossing points. The amplitude modulation of the oscillations is slightly different for each step. Some steps have nodes close to the middle of the step while others are closer to one of the sides, at about a third or two thirds of the step. The evolution is closely periodic and symmetric under a reflection at $\Phi = 6\pi$. Although they are very small in the plot, we also gain components in the $\pm i$ states of the itinerant sub-bands when their energies cross the energies of the S states. It is the S states that lose component when the $\pm i$ states gain it. Still, these components are very minor, so the localized component is $|\Psi_{\text{loc}}|^2 \approx 1 - 2|\Psi_{S_+}|^2$. The S state components are still very small so the state is mainly localized.

In Fig. 4.2a, $(-y_0, x_0) = (4.3, -0.84)$, we are representing the itinerant component $|\Psi_{\text{it}}|^2 = 1 - |\Psi_{\text{loc}}|^2$ (It) as a substitute for the localized component so that its size is always comparable to the itinerant components. It is, obviously, the biggest component in this plot. Here we have a case where the state is able to lose a big portion of its localized component to the S components, up to 70%. The period of the step-like behaviour is also bigger than in 4.1d, and the components seem to increase and decrease similarly to a crest of a sine function. The S components in the latest steps have considerable noise. This is due to the loss in component to the rest of the itinerant states that, although it is tiny, accumulates during long simulations, increasing the noise in the latest steps. However, the localized (itinerant) component seems unaffected by this noise. It is also noticeable that there is a slight difference between the two components of the S states, which did not occur in the previous simulations, and there is also a varying phase difference between both components, which creates an additional amplitude modulation of the localized component through, similar to beats. When there is a π phase difference, marked with arrows, the oscillations cancel when summed and the localized component has nodes in the amplitude of the oscillations. These nodes are different from the ones in 4.1d since there was no phase difference between S components in that case, and those nodes were present in the S components already, not only on the localized component.

In Fig. 4.2b, $(-y_0, x_0) = (7.31, -1.42) = 1.7 \times (4.3, -0.84)$, we observe a similar step-like behaviour to the one in Fig. 4.2a. The main differences are the smaller maximum itinerant component reached, 10%, and the amplitude modulation. The oscillation amplitude has a very noticeable evolution from step to step: starting with a uniform amplitude in the first step, it then starts to thin at the left side until it creates a node at that side. The node then advances until it reaches the right side of the step. Also, the itinerant components start to decrease when the node surpasses the middle of the

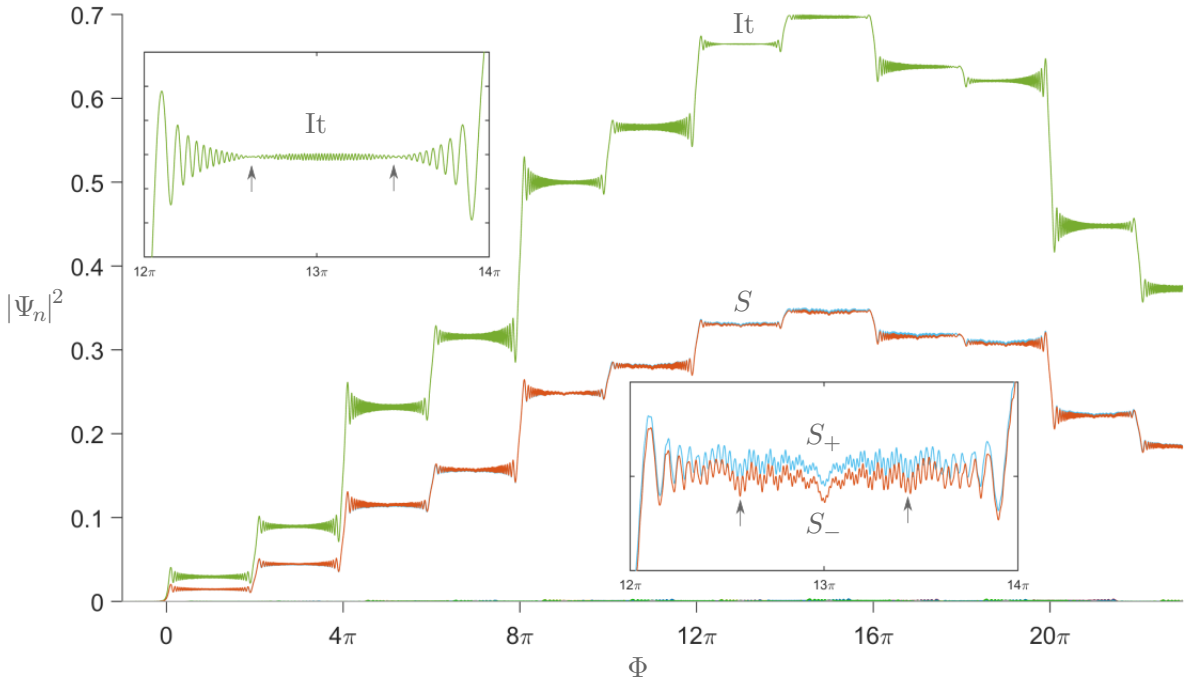

(a) $(-y_0, x_0) = (4.3, -0.84)$.

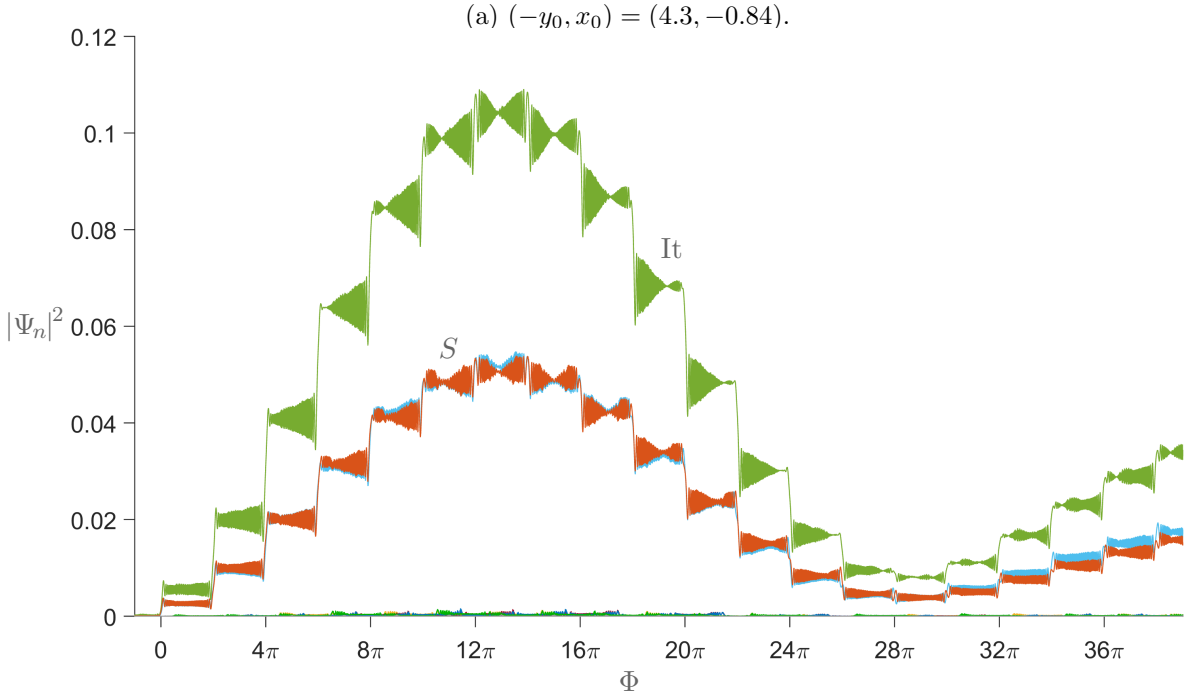

(b) $(-y_0, x_0) = (7.31, -1.42)$.

Figure 4.2: More simulations on the 2×2 Lieb lattice, for a localized state that started as $|L_+(-\pi)\rangle$ (Eq. 3.48) and for two different uniform electric fields.

step. The oscillation amplitude after $\Phi = 28\pi$ is more complicated mainly due to an increased asymmetry between S components and to the phase difference effect we saw in the previous figure. Now, the uniform electric field used is 1.7 times the one in the previous simulation. Remember from section 3.4 that the transition element between S and localized states, in the 2×2 lattice, is proportional to the uniform electric field. However, by increasing the field we obtained smaller step jumps and a smaller maximum itinerant component, and also different oscillation amplitudes. These simulations show that, when considering the step-like behaviour, ignoring all the itinerant states except for the S states and reducing the system to the flat band together with the S states, like in Eq. 3.47, is a very good approximation, but this small system can still be very non-linear. While one very important element of D has a linear behaviour with the electric field, increasing or decreasing that element linearly does not entail a linear response from the overall system of differential equations since there are other relevant elements, the ones pertaining to the internal rotation, who depend only on our choice of localized basis.

In the first simulations there was perfect symmetry between $\pm E$ components, but in Figs. 4.2a and 4.2b we saw the two S components separate in both amplitude and oscillation phase, meaning the energy of the state is not zero in the latter case. From all the symmetries found between states of opposite energy, it could be expected that the evolution would also be perfectly symmetric. That is not the case when the elements of D have time dependent phase terms (constant phases can generally be absorbed by the states and do not have an effect). Still, there is a basis of states where the matrix D of the 2×2 lattice is a real matrix, as we saw at the end of section 3.3.1, and the phase $-i$ that multiplies the Hamiltonian in the evolution equation can be absorbed by the states, as we shall see later, so time dependent phases are not the cause for the asymmetry. The cause is that there are already phase differences present in the initial state. The full evolution matrix in the reduced sub-space of the 2×2 lattice (Eq. 3.47) is

$$\begin{pmatrix} -iE & f & 0 & 0 & 0 \\ -f & 0 & a & 0 & f \\ 0 & -a & 0 & b & 0 \\ 0 & 0 & -b & 0 & 0 \\ 0 & -f & 0 & 0 & iE \end{pmatrix}. \tag{4.3}$$

In Fig. 4.1c the initial state, in the same basis that the evolution matrix is written, is $\Psi_0 = (0, 0, 1, 0, 0)$, since it is the two-plaquette state that does not rotate with S for the uniform electric field chosen, so the evolution is perfectly symmetrical. In Fig. 4.1d the initial state is $\Psi_0 = (0, 1, 0, 0, 0)$, the state that does rotate with S, and we have symmetry again. In Figs. 4.2a and 4.2b the uniform electric field is not in a diagonal, so the state that rotates with S is a combination of the two two-plaquette states. The initial state will be $\Psi_0 = (0, z_1, z_2, 0, 0)$, for some combination of complex numbers z_i with a relative phase between them. That relative phase will then cause the asymmetry in the evolution.

4.2.2 Six by six lattice

We shall now see simulations on the 6×6 lattice to better understand how the phenomena found in the 2×2 lattice, which is an especially simple case, scale with the size of the lattice. The color-code of the closest sub-band states and of the itinerant (localized) component is maintained. For bigger lattices we may put our two-plaquette initial state $|L_+\rangle$ in many places.

In Fig. 4.3a, $(-y_0, x_0) = (0, 0)$, we placed $|L_+\rangle$ in the middle of the lattice. Like in Fig. 4.1b, we only have components in $\pm i$ states, indicating that the two-plaquette state in the middle of the lattice is a combination of $\pm i$ zero energy states. This is easy to see analytically since the 2×2 lattice is a sub-lattice of the 6×6 lattice, and the 2×2 localized states will be localized states of the 6×6 lattice, so the $\pm i$ localized states of the 2×2 centred in the lattice will be $\pm i$ states of the 6×6 lattice, and therefore the two-plaquette state is still a combination of $\pm i$ states. The same could not be said if the two-plaquette state was not centred in the lattice. The itinerant components increase when the energy difference diminishes, which happens close to $\Phi = 2\pi n$ (see Fig. 2.8b for reference. The 8×8 and 6×6 energy diagrams are very similar). Opposite energy components are equal, possibly indicating the matrix D is real, at least for $|\boldsymbol{E}_0| = 0$. The evolution is not as simple and periodic as it was in 4.1b.

In Fig. 4.3b, $(-y_0, x_0) = (0, 0)$, we placed $|L_+\rangle$ at a corner of the lattice. We separated the full itinerant component in another plot for better visibility. The state now gains components in all itinerant states, so the initial state has a projection in states of all possible rotation phases. We now have itinerant component for all flux. There are still peaks of $\pm i$ components close to $\Phi = 2\pi n$ like in 4.3a, although they are smaller, but the ±1 itinerant components have a minimum in that region and reach their maximum not when the energy is at its closest to zero, the crossing points, but somewhere inside each 2π interval. This is easier to understand when we remember that the S to localized transition element is zero at $\Phi = 2\pi n$ for larger than 2×2 lattices and for zero uniform electric field (Eq. 3.58), so the amplitude of the S component is suppressed at the crossing points.

In Fig. 4.3c, $(-y_0, x_0) = (2.21, 5.72)$, we placed $|L_+\rangle$ in the middle of the lattice. The main thing of note is the return of the steps. At the crossing points, the S components increase, but that is quickly lost to the other itinerant states whenever the energy of the S states cross or get close to the other states, which happens very frequently since the energies in each sub-band are tightly interlaced (Fig. 2.8c). This means whenever we arrive at another crossing point after we have already gone through one, the state has lost most of its S component, so the localized component will most likely decrease again since the maximum it can increase is the sum of the S components. This means the state is always losing localized component whenever it crosses the S states, which then subsequently lose to localized states that are further away in energy, and so on, in a process that resembles diffusion. We can try to reduce the diffusion effect by slowing down the increase of magnetic field (smaller ω). For non-zero uniform electric field, no major difference was identified between time evolutions with different starting positions of the two plaquette state.

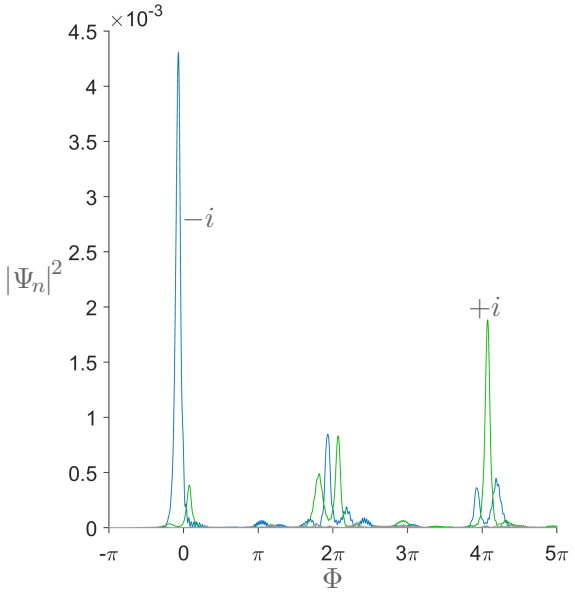

(a) $(-y_0, x_0) = (0, 0)$.

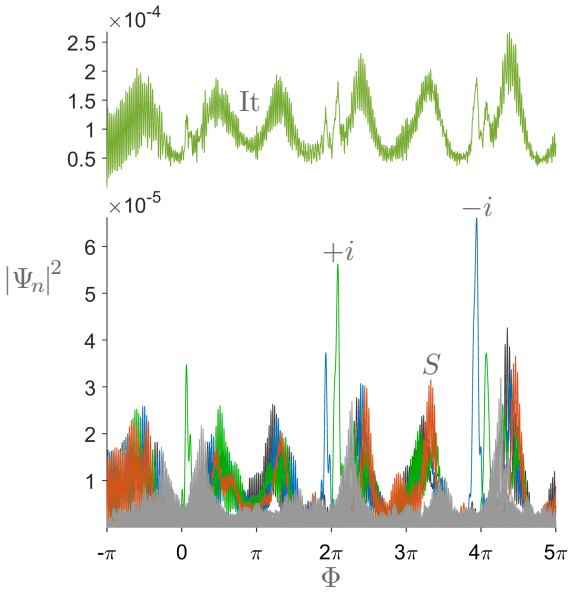

(b) $(-y_0, x_0) = (0, 0)$.

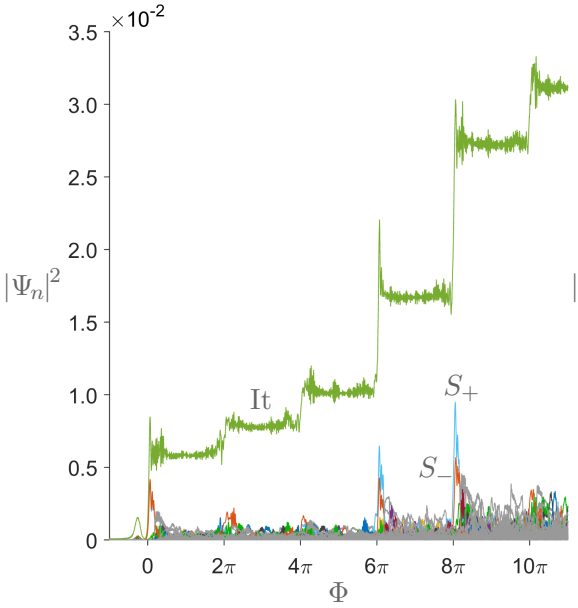

(c) $(-y_0, x_0) = (2.21, 5.72)$.

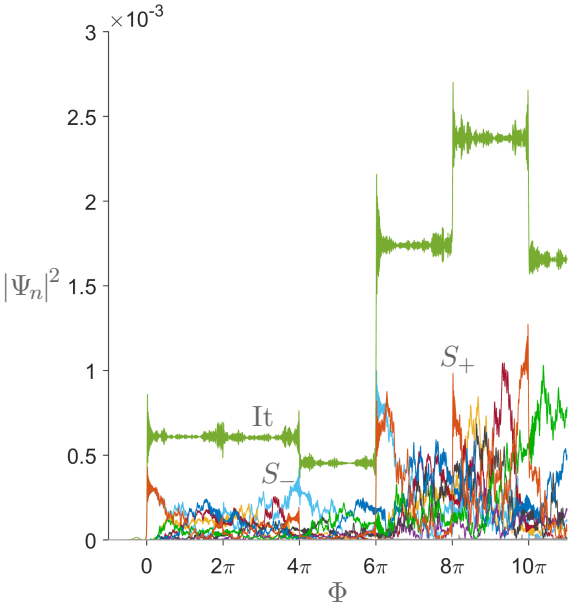

(d) $(-y_0, x_0) = (2.21, 5.72)$.

Figure 4.3: Results of simulations on the 6×6 lattice for a localized state that started as $|L_+(-\pi)\rangle$ (Eq. 3.48) (a,c,d) in the middle of the lattice and (b) at a corner of the lattice, for (c) $\omega = 0.01$ and (d) $\omega = 0.001$.

In Fig. 4.3d, $(-y_0, x_0) = (2.21, 5.72)$, we are using $\omega = 0.001$, ten times smaller than previously, and again we placed $|L_+\rangle$ in the middle of the lattice. We still have steps, of smaller height, and the oscillation frequency has increased. The transitions between steps are narrower in Φ and the steps are better defined. The itinerant component no longer disperses into the bulk of itinerant states, remaining mainly in the eight closest sub-band states. The diffusion inside these sub-bands still prevails, which reduces the S components and therefore interferes with the step pattern, but the reduction is smaller than previously and now we see some step transitions where localized component is gained. One thing to note in these last two simulations is the more accentuated asymmetry between opposite energy states. This is due to the matrix D having time dependent phase terms when $L > 2$. Still, the symmetries are expected to manifest in that for each localized state there should be another, similar, localized state whose time evolution is symmetric to the first one by $E \to -E$.

4.3 Step-like behaviour

From the simulations we may conclude that significant transitions between states occur only when the difference of energy between the states is sufficiently small. The terms to compare in transitions from and to localized states are $\Delta E = E - 0$ and $\langle E'|L\rangle$. When $\Delta E \gg \langle E'|L\rangle$, the transition does not occur and each component has an oscillatory behaviour. The terms $\langle E'|L\rangle$ are proportional to electric field integral terms, which in turn are proportional to ω, $\langle E'|l\rangle = \omega \frac{d\langle E|}{d\Phi} |L\rangle$, so for a very slow evolution only when $\Delta E \approx 0$ can the transition occur. The only itinerant states that reach that condition are the S states and only very close to the crossing points. However, as we increase the size of the lattice so will the density of states increase and the energy difference between localized states and itinerant states apart from the S states will reduce. For the infinite lattice, a finite ω will make a fraction of the itinerant band accessible. For the lattice sizes we are using we do not have to consider this hypothesis. We can see the dependence on ω better with the time evolution equation written as

$$\frac{d\mathbf{\Psi}_\Phi}{d\Phi} = (-i\frac{H_\Phi}{\omega}(t) + D_\Phi)\mathbf{\Psi}_\Phi, \tag{4.4}$$

where $(D_\Phi)_{ij} = \frac{d\langle E_i|}{d\Phi} |E_j\rangle = D_{ij}/\omega$. The matrices H_Φ and D_Φ are independent of the rate of flux change. When $\Delta E \gg \omega$, the first matrix dominates the time evolution which results in oscillation terms related to the energy (of the kind of $\exp -i \int E_+(t)dt$) dominating. When $\Delta E \ll \omega$, the matrix D dominates. It is important to note that the small oscillations do not stem only from the exponential phase terms like $\exp -i \int E(t)dt$, since phase terms do not appear in $|\Psi_\Phi|^2$. The oscillations are a combination of the energy phase terms and small contributions of the matrix D, which can be seen as a perturbation matrix in that regime. It is noticeable how the oscillations decrease in amplitude as ΔE increases: in the limit of very large ΔE, the solution would be the trivial one and $|\Psi_\Phi|^2$ would be constant.

In the 2×2 lattice, the S to localized transition is proportional to the uniform electric field for any flux, so it follows directly that the step-like behaviour only occurs for non-zero uniform field, but for larger lattices the electric field dependence is more complicated. However, when $|\boldsymbol{E}_0| = 0$ the transition term goes to zero exactly when the energy also goes to zero, at $\Phi = 2\pi n$ (Eq.3.58), so there may not be an interval where $\langle S'|L_S\rangle > \Delta E$, and the step-like behaviour will be suppressed, if it exists at all. From the simulations we can say that the step-like behaviour, which is the main source of loss of localized component, is dependent on the existence of a uniform electric field.

Chapter 5

Three level system

In this chapter we study a three level system that features the step pattern found in the Lieb simulations. When the matrix elements are real, the system can be interpreted as a classical precession system. When the elements have time dependent phases a beat interference pattern appears in the localized component. We are able to replicate Lieb simulation results through an adequate choice of matrix elements.

The most relevant itinerant states in the evolution of localized states are the two that cross them, the S states. Apart from those two, the localized states also rotate with each other, like in Eq.4.3, and there is not an energy difference that suppresses the transition between them since they all have the same energy, like in Eq. 4.3, so there are always uninhibited transitions between localized states. Still, in our time evolution we are not interested in the components over time in each localized state, only on the total localized component, so we propose a system of three states, the two S states and a localized state that will represent the whole localized subspace. The evolution equation of a state Ψ in this system is

$$\frac{d}{dt}\begin{pmatrix}\Psi_+\\ \Psi_0\\ \Psi_-\end{pmatrix} = \begin{pmatrix}-iE & f & 0\\ -f^* & 0 & f^*\\ 0 & -f & iE\end{pmatrix}\begin{pmatrix}\Psi_+\\ \Psi_0\\ \Psi_-\end{pmatrix}, \tag{5.1}$$

for some complex function $f(t) \propto \omega$. We could have eliminated one of the S states as a further simplification, but the fact that the system has three components allows us to give it an interesting geometrical interpretation, as we shall see. Now, f can not be $\langle S'_+|L_S\rangle$ if this system is to effectively represent a system like 4.3. In that case, we would be considering that the other localized states do not exist. For this system to account for the S to localized term and for the internal rotation of the localized states, f has to be a function of all the elements of D that are missing in this system: $\langle S'_+|L_S\rangle$, the internal rotations, and also the initial state Ψ_0, particularly the initial configuration on the localized subspace. f is then an effective function that condenses in it the full interaction between the S states and the localized subspace. We will not try to show how one would build such a function analytically. It is not known if that is even possible. We will only see how we can guess what function it is by looking at the simulation results. Let us first analyse further the system so as to better understand it.

5.1 Classical precession system

The S states can be written as $|E_\pm\rangle = (|A\rangle \pm i\,|BC\rangle)/\sqrt{2}$, where both $|A\rangle$ and $|BC\rangle$ are real at $\Phi = 0$. Performing the basis change $\{x = (\Psi_+ + \Psi_-)/\sqrt{2}, z = i(\Psi_- - \Psi_+)/\sqrt{2}, y = \Psi_0\}$, and defining $g = -i\sqrt{2}f$, we have

$$\frac{d}{dt}\begin{pmatrix} x \\ y \\ z \end{pmatrix} = \begin{pmatrix} 0 & 0 & E \\ 0 & 0 & -g^* \\ -E & g & 0 \end{pmatrix}\begin{pmatrix} x \\ y \\ z \end{pmatrix}, \tag{5.2}$$

where (x, y, z) will correspond to components in $\{|A\rangle, |L\rangle, |BC\rangle\}$ respectively. If g were real, the system would become real. More so, it would be a classical precession system of the position vector $\boldsymbol{r} = (x, y, z)$ in the unit sphere,

$$\frac{d\boldsymbol{r}}{dt} = (g, E, 0) \times \boldsymbol{r} = \boldsymbol{\Omega} \times \boldsymbol{r}. \tag{5.3}$$

Let us use for now g real. It is still an interesting case since it applies to the 2×2 lattice well. We shall see later the general case. In general, the precession vector $\boldsymbol{\Omega}$ changes its magnitude and orientation over time. At each time the position vector is rotating around $\boldsymbol{\Omega}$ with instantaneous angular velocity $\Omega = \sqrt{E^2 + g^2}$. The system has exact solution for constant $\boldsymbol{\Omega}$, which is

$$\begin{aligned} x &= \frac{1}{\Omega}\left(gc - E\sqrt{1-c^2}\cos(\Omega t + \theta_0)\right), \\ y &= \frac{1}{\Omega}\left(Ec + g\sqrt{1-c^2}\cos(\Omega t + \theta_0)\right), \\ z &= \sqrt{1-c^2}\sin(\Omega t + \theta_0), \end{aligned} \tag{5.4}$$

with an initial phase θ_0 and $c = (\boldsymbol{\Omega}\cdot\boldsymbol{r})/\Omega$, $-1 \le c \le 1$, a constant quantity. The localized component $|y|^2$ will oscillate with frequency Ω and amplitude $\sim g^2/\Omega^2$. This oscillation is due to the precession axis not matching the zero energy axis $\hat{y}$. If g were zero, the position vector would still precess, but this time around $\hat{y}$, maintaining the angle with that axis constant, and consequently the y component would also be constant.

The equations 5.4 may be adapted to fit a situation of varying energy. Consider that $E = E_0 \sin(\omega t/2)$, closely matching the energies of the S states, and that we are in the region where $E \gg g$, away from the transition regions. The instantaneous angular velocity is then $\Omega = \frac{d\theta}{dt} = \sqrt{E^2 + g^2} \approx E$. From these three equalities we obtain $\theta = \theta_0 + \int_0^t E(t')dt' = \theta_0 - 2E_0\cos(\omega t/2)/\omega$, so the sinusoidal function that has instantaneous angular velocity E is $\cos(-2E_0\cos(\omega t/2)/\omega + \theta_0)$. Substituting the cosine and the energy in the equation of the localized component y in 5.4 we obtain

$$y = c\frac{E_0}{\Omega}\sin\frac{\omega t}{2} + \sqrt{1-c^2}\frac{g}{\Omega}\cos\left(-\frac{2E_0}{\omega}\cos\frac{\omega t}{2} + \theta_0\right). \tag{5.5}$$

In Fig. 5.1a we show the S components and their sum over time from a simulation of Eq. 5.2 with $g = \omega = 0.01$, $E = \sin(\Phi/2)$, $\Phi_0 = -\pi$ and $\Psi_0 = (0, 1, 0)$, with $\Phi = \omega t$. We can

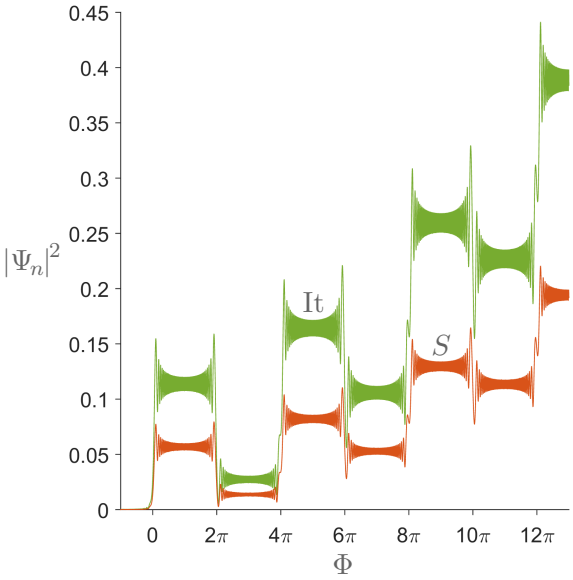

(a) $g = 0.01$.

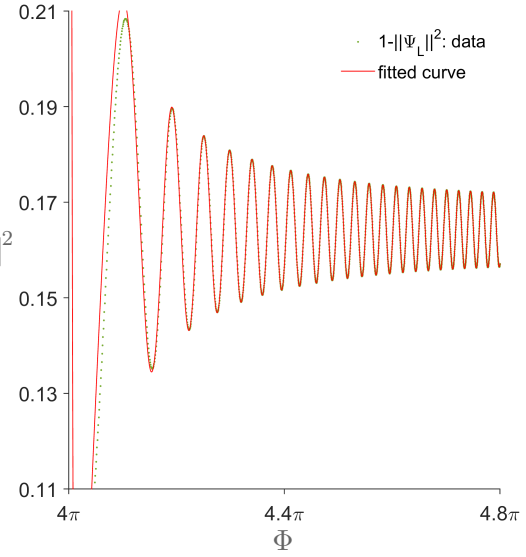

(b) $g = 0.01$.

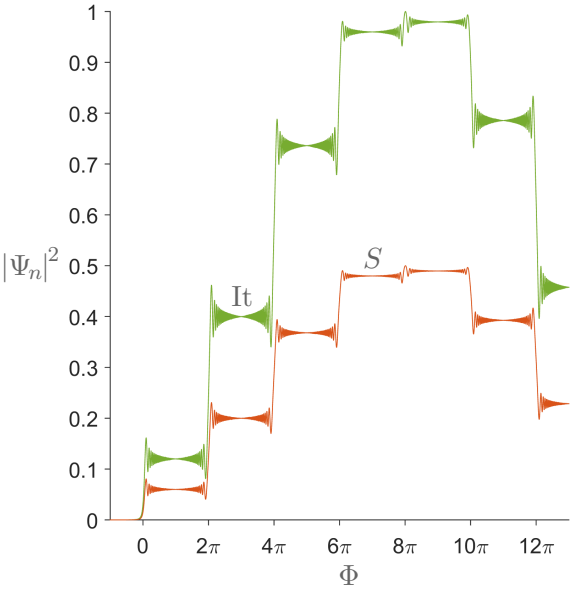

(c) $g = 0.01\cos(0.01t/2)$.

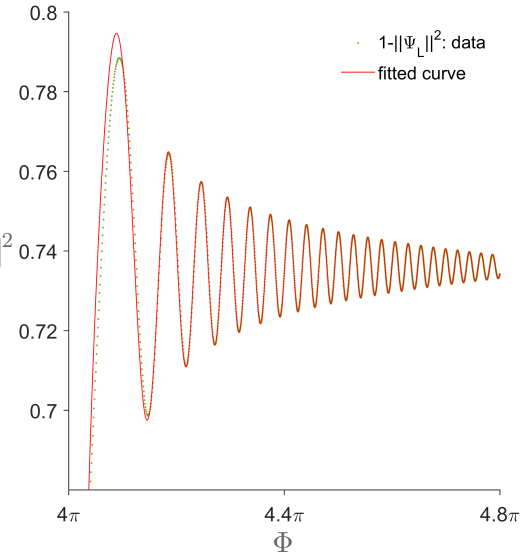

(d) $g = 0.01\cos(0.01t/2)$.

Figure 5.1: (a,c) Simulations of the three level model of Eq. 5.2 with $\omega = 0.01$, $E = \sin(\omega t/2)$, $\Phi_0 = -\pi$, $\Psi_0 = (0, 1, 0)$, for two different g functions. (b,d) Fits of steps in the simulations on the left using as fitting function Eq. 5.5.

identify the step pattern that we saw in the Lieb simulations. The two S components are equal. In Fig. 5.1b we show the fit of the third step with Eq.5.5, which, for some c and θ_0, fits the oscillations extremely well in the region where $E \gg g$.

In Fig. 5.1c, we have the same simulation as in Fig. 5.1a except with $g = \omega \cos(\omega t/2)$, $\omega = 0.01$. The Eq. 5.5 is still an approximate solution for a general real function g (remember that Ω is a function of g too) in the $E \gg g$ region, meaning we may use a time dependent g in the equation, like we did in Fig. 5.1d. This way we see that g/Ω approximately modulates the amplitude of the oscillations, and the nodes we see in 5.1c coincide with the nodes of g.

We can also see one of the effects that g has on the step transitions with these last two simulations. A constant g (Fig. 5.1a) created a pattern of steps that alternates between rising and lowering the steps. A function g that alternates in sign at each crossing point $\Phi = 2\pi n$ (Fig. 5.1a) makes the steps repeatedly rise or fall.

In the precession model the step-like transitions and the oscillations gain geometrical interpretations. It becomes a competition between precessions around two different axes. We may picture the time evolution like this: let us start at the maximum of energy, where the state precesses around an axis that is almost the $\hat{y}$ axis so that we only see very small oscillations around an average value that is the radius of precession. When the energy, as it slowly decreases, goes through zero, $\mathbf{\Omega}$ becomes for a short period of time a vector whose main component is in the $\hat{x}$ axis, so, during that time, the position vector will rotate a bit in the $y0z$ plane, effectively increasing or decreasing the precession radius around the $\hat{y}$ axis, and therefore altering slightly the component in the localized states.

5.2 Complex transition element

If $g(t)$ is complex only because of a constant phase term, that phase can be absorbed into the localized state by a redefinition of $y = \Psi_0$, so we would obtain the same results. A general complex function $g(t) = u(t)e^{i\theta}$ will still exhibit the same step-like behaviour, and $|g(t)| = u(t)$ will still play a role in the modulation of each step, but the phase term $e^{i\theta}$ will cause phase and amplitude differences between the two S states, which in turn creates an additional modulation of the oscillations of the localized component through the interference of the S components. In Fig. 5.2a we have a step of the evolution for $g = \omega \cos(\Phi)$. The $\cos(\Phi)$ modulation is noticeable, creating nodes at $\pi/2$ and $3\pi/2$. The modulation is present and equal in the three components, and the two S components are equal. In Fig. 5.2b we used $g = \omega \cos(\Phi)e^{i\Phi/2}$. The two S components have slightly different amplitudes even though the initial state was purely localized. The modulation of the two is given by $\cos(\Phi)$ while the localized component has an extra node at π. This node is due to a π phase difference at $\Phi = \pi$ between the oscillations of the S components. The phase term causes a varying phase difference between S states, which in turn causes an additional modulation of the localized component due to the beat interference patterns. The full amplitude modulation of the localized component is given by the real part of g, which in this case is $\mathrm{Re}(g) = \omega \cos(\Phi) \cos(\Phi/2)$.

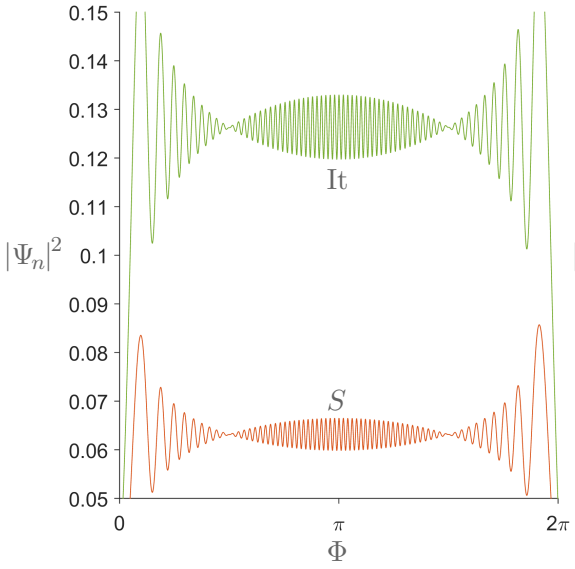

(a) $g = \cos(\omega t)$.

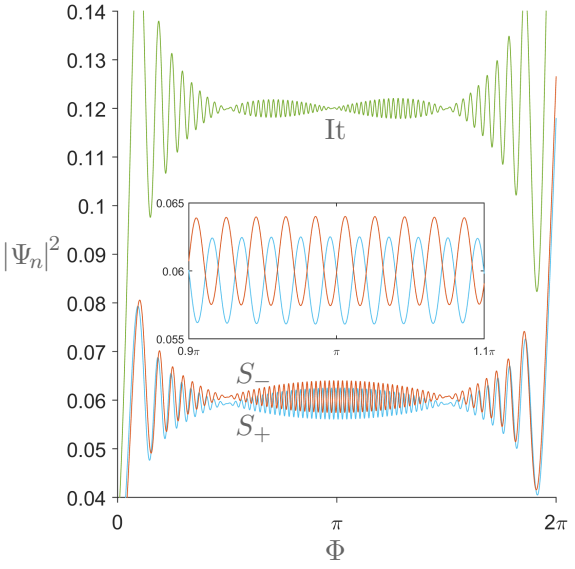

(b) $g = \omega \cos(\omega t) e^{i\omega t/2}$.

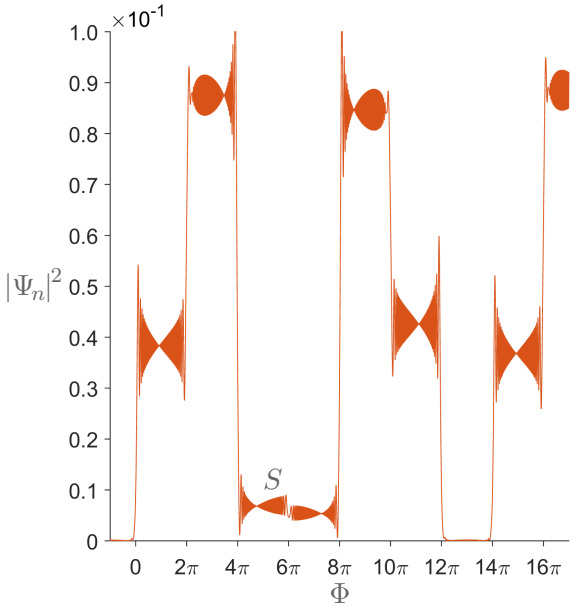

(c) $g = \sin(1.57\omega t/2 - 2.27)$.

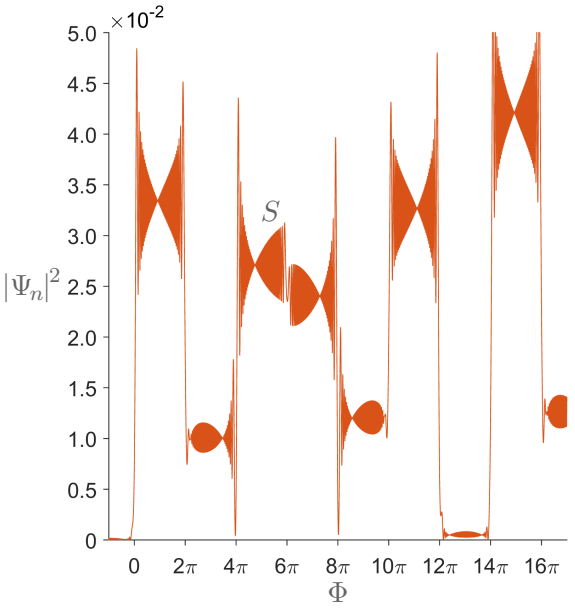

(d) g in Fig. 4.1d.

Figure 5.2: Results of simulations of the three level model of Eq. 5.2 with $\omega = 0.01$, $E = \sin(\omega t/2)$, $\Phi_0 = -\pi$, $\Psi_0 = (0, 1, 0)$ for different g. In (a,b) only a step is shown. In (b) we show a close-up of the π phase difference region. The simulations in (c,d) resemble the Lieb simulation results in Fig. 4.1d.

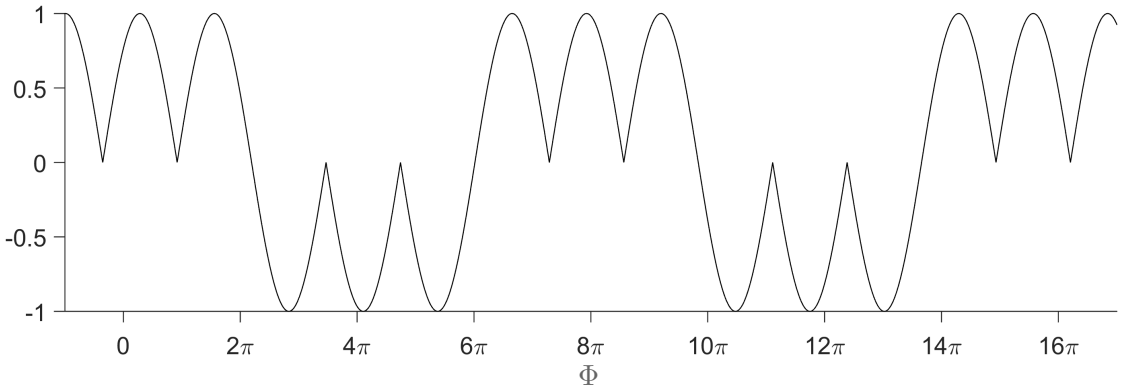

Figure 5.3: The function $g(\Phi)$ used in the simulation shown in Fig. 5.2d.

5.3 Reproduction of Lieb results

Let us try to reproduce the results of a Lieb simulation using the three level model, in particular, the simulation shown in Fig. 4.1d. To do this we must find an effective rotation function g that is appropriate for this simulation. This simulation has perfect symmetry between $\pm E$ components, so we may use a real g. The elements of D are most likely all periodic with the same period as the energies, 4π or 2π, but g, the combination of several elements of D, does not have to be periodic, or it may have a different period. As we saw previously, the nodes in the S components coincide with nodes of $g(t)$. The nodes in the simulation are equidistant, which suggests that g may be a sinusoidal function, $g = \sin(\mu\Phi/2+\theta_0)$, for some constant factor μ and initial phase θ_0. We can determine those constants using two nodes Φ_1 and Φ_2 of the simulation:

$$\mu\Phi_1/2 + \theta_0 = n_1\pi, \quad \mu\Phi_2/2 + \theta_0 = n_2\pi. \tag{5.6}$$

We may choose $n_1 = 0$ by a redefinition of the initial phase. Solving the system we have

$$\mu = \frac{2\pi(n+1)}{\Phi_2 - \Phi_1}, \quad \theta_0 = -\frac{\mu\Phi_1}{2}, \tag{5.7}$$

where n is the number of nodes between nodes Φ_1 and Φ_2. For example, the S Lieb component has nodes at 0.92π and 4.74π, with two other nodes between those two, which gives us $\mu = 1.57$ and $\theta_0 = -2.27$. In Fig. 5.2cm we simulated the three level system with $g = \sin(1.57\Phi/2 - 2.27)$. The step pattern is similar to the one in 4.1d. The nodes and amplitude modulation seem correct, but some step transitions are in the wrong direction. The four steps between $\Phi = 2\pi$ and 10π are inverted. As we saw in Figs. 5.1a and 5.1c, the sequence of signs of g at the crossing points influences how the steps rise and fall. We can change the step pattern by using another pattern of crests and troughs, instead of the crest-trough-crest of the sine function. The function will then be $g = s(\Phi)|\sin(1.57\Phi/2 - 2.27)|$, for some sequence of $s = \pm 1$, crests and troughs. The sequence that correctly emulates the Lieb results is three crests-three troughs repeatedly,

as shown in Fig. 5.3. The simulation for this g is in Fig. 5.2d. The step pattern of this three level model simulation and of the Lieb simulation are almost identical.

In a $L > 2$ system, not only does the number of localized states increases, but the transitions between itinerant states of the same sub-band are very important, so the itinerant states of the three level model must represent not only the S states but itinerant sub-band. This means g will take into account an increasingly high number of elements of D. The step oscillations are much more complex because of this, as we can see in Figs. 4.3c and 4.3d. Finding a function g that correctly replicates results of an $L > 2$ simulation by examining the nodes is not possible. Still, for any Lieb time evolution of any L there should be a function g that replicates the evolution of the localized component.

Chapter 6

Conclusions

We have studied the slow time evolution of localized states of the Lieb lattice with increasing magnetic flux. A curious step pattern of the localized component has been found and we have shown that this behaviour can be interpreted as a precession movement of the evolving state around a time dependent vector.

The bipartite property of the Lieb lattice implies the $\pm E$ symmetry and that non-zero energy eigenstates have equal occupation in each sub-lattice, which in turn does not allow the flat band states to gain energy for any flux, except for the two S eigenstates. We revealed the importance of the electric field in the time evolution, and how its invariance compared to the invariance of the Lieb eigenstates affects the time evolution. The fact that the S to localized state transition term is proportional to the uniform electric field at $\Phi = 2\pi n$ is very important in understanding when the step pattern from chapter 4 occurs or, equivalently, to what extent localized states are robust against time dependent magnetic fields. The three level model from chapter 5 helped us understand the step pattern and interpret the Lieb time evolution in terms of a classical precession, which reduces the complexity of the system considerably. The fact that we can very effectively replicate Lieb simulations with this system implies an interesting mathematical result: that there is an n-dimensional system of differential equations with the same solution to one of its components than a bigger m-dimensional system with all equations coupled. Sometimes, the construction of the smaller system is easier.

Although the focus of this thesis was in the Lieb lattice, part of the formalisms and results are very general and could be adapted to fit other systems. For example, the formalism in section 3.2 is applicable to any discrete states system. The calculations regarding what transitions are allowed depending on the electric field in subsection 3.2.1 can be adapted and used in a system with other physical invariances and other electric fields. We can also retrieve some general results. For example, we can say that if a physical system is invariant under a physical transformation $\hat{T}$ and we then apply an electric field that is also invariant under $\hat{T}$ (meaning the overall invariance of the system will not have changed), only transitions between states of equal $\hat{T}$ invariance phase, which is the eigenvalue of the state on $\hat{T}$, are allowed. This is the case when we apply only the circular electric field to the Lieb lattice. Any other electric field that was C_4

invariant would have the same effect. The basis freedom from section 3.3 is also true for any subspace that remains degenerate over time.

As seen on the time evolution simulations and explored in section 4.3, the appearance of steps of the localized component in the Lieb lattice is dependent on the existence of a uniform electric field component, or, more generally, the existence of an electric field component not invariant under $\hat{R}_{\pi/2}$ rotations. We can expect the steps to appear in slow time evolutions of other systems if certain conditions are met: if, from time to time, the energies of two or more eigenstates get sufficiently close or even cross each other so that the transition term $\langle E_i'|E_j\rangle$ dominates over the energy term for a small period of time, then there will be significant and permanent transitions between those states. Of course, if the energy difference does not go to zero, we can always slow the evolution further by reducing ω so that the transition term becomes much smaller than the minimum energy difference and there will not be a permanent exchange in component. The same can not be done if the energy difference is zero at some point.

We can picture the quasi-adiabatic time evolution of any discrete state system as follows: as long as the energies of two or more eigenstates do not meet, there is no change in the $|\Psi_n|^2$ components of the evolving state. When at least two energies become equal and at least one of those eigenstates is occupied by Ψ, there is an exchange in occupation proportional to the transition element at the point the energies meet, $\langle E_i'|E_j\rangle\,(E_i = E_j)$. The Lieb lattice under a magnetic field is a system of variable energy gap between bands. When the energy gap periodically goes to zero, the electrons are able to change their occupation on each band. In any system that exhibits a variable gap between bands under a quasi-adiabatic time evolution, the electrons will be able to change bands when the gap closes and if there is an applied electric field. Depending on the system, said field may have to reduce the symmetry of the system for the transition to occur, that is, for $\langle E_i'|E_j\rangle\,(E_i = E_j)$ to be different than zero, as it happens in the Lieb lattice.

The step pattern may be observed in Lieb optical lattices under time dependent perturbations. In photonic Lieb lattices it is possible to create a photonic state that is localized.[19,20] Application of a magnetic field would have no effect, but there may be a perturbation of the waveguides that serves as a substitute of the magnetic field, possibly some spatially dependent perturbation of the refraction index. However, that perturbation must not break the flat band, just like the magnetic field. A perturbation of the waveguide that changes over its length is, from the standpoint of the photonic state that travels the waveguide, a time dependent perturbation, so it may be possible to replicate a time dependent magnetic field, and by making the perturbation periodic we will periodically go through a crossing point. By measuring the light intensity at an A (site) waveguide over its length, we are approximately measuring the itinerant component over time. If the perturbation correctly replicates the magnetic field, then, if the perturbation does not reduce the C_{4v} symmetry, the loss of localized component should be minimal, while if the symmetry is reduced to C_4 a step pattern should appear. However, such a perturbation is only theorized here, and it is not known if it exists.

The $\pm E$ symmetry due to the bipartite property of the lattice has as a consequence a separation of sub-lattices when considering $\hat{H}^2$, as seen in subsection 2.5.1. The sep-

aration reveals a relation between the energies and eigenstates of the Lieb, square and Mielke lattices. It would be interesting to explore this property further and possibly apply it to other bipartite lattices in the future.

Bibliography

[1] M. Nita, B. Ostahie, and A. Aldea. Spectral and transport properties of the two-dimensional Lieb lattice. *Phys. Rev. B*, 87:125428, Mar 2013.

[2] A Mielke. Exact ground states for the Hubbard model on the Kagome lattice. *J. Phys. A-Math. Gen.*, 25(16):4335, 1992.

[3] Petra Pudleiner and Andreas Mielke. Interacting bosons in two-dimensional flat band systems. *The European Physical Journal B*, 88(8):1–8, 2015.

[4] Hal Tasaki. Ferromagnetism in the Hubbard models with degenerate single-electron ground states. *Phys. Rev. Lett.*, 69(10):1608–1611, Sep 1992.

[5] R. G. Dias and J. D. Gouveia. Origami rules for the construction of localized eigenstates of the Hubbard model in decorated lattices. *Scientific Reports, 16852*, 2015.

[6] Sergej Flach, Daniel Leykam, Joshua D. Bodyfelt, Peter Matthies, and Anton S. Desyatnikov. Detangling flat bands into fano lattices. *EPL (Europhysics Letters)*, 105(3):30001, 2014.

[7] A. A. Lopes and R. G. Dias. Interacting spinless fermions in a diamond chain. *Phys. Rev. B*, 84:085124, Aug 2011.

[8] Elliott H. Lieb. Two theorems on the Hubbard model. *Phys. Rev. Lett.*, 62(10):1201–1204, Mar 1989.

[9] K. Kusakabe and H. Aoki. Ferromagnetic spin-wave theory in the multiband hubbard model having a flat band. *Phys. Rev. Lett.*, 72:144–147, Jan 1994.

[10] Andreas Mielke. Ferromagnetism in Single-Band Hubbard Models with a Partially Flat Band. *Phys. Rev. Lett.*, 82(21):4312–4315, May 1999.

[11] Kazuto Noda, Kensuke Inaba, and Makoto Yamashita. Flat-band ferromagnetism in the multilayer lieb optical lattice. *Phys. Rev. A*, 90:043624, Oct 2014.

[12] J.D. Gouveia and R.G. Dias. Magnetic phase diagram of the Hubbard model in the Lieb lattice. *Journal of Magnetism and Magnetic Materials*, 382(0):312 – 317, 2015.

[13] K. C. Rule, M. Reehuis, M. C. R. Gibson, B. Ouladdiaf, M. J. Gutmann, J.-U. Hoffmann, S. Gerischer, D. A. Tennant, S. Süllow, and M. Lang. Magnetic and crystal structure of azurite $cu_3(co_3)_2(oh)_2$ as determined by neutron diffraction. *Phys. Rev. B*, 83:104401, Mar 2011.

[14] V. J. Emery. Theory of high-T_c superconductivity in oxides. *Physical Review Letters*, 58:2794–4797, 1987.

[15] R. T. Scalettar, D. J. Scalapino, R. L. Sugar, and S. R. White. Antiferromagnetic, charge-transfer and pairing correlations in the three-band Hubbard model. *Physical Review B*, 44:770–781, 1991.

[16] Hiroyuki Tamura, Kenji Shiraishi, and Hideaki Takayanagi. Ferromagnetism in Semiconductor Dot Array. *Jpn. J. Appl. Phys.*, 39:L241, 2000.

[17] Naoyuki Masumoto, Na Young Kim, Tim Byrnes, Kenichiro Kusudo, Andreas Löffler, Sven Höfling, Alfred Forchel, and Yoshihisa Yamamoto. Exciton-polariton condensates with flat bands in a two-dimensional kagome lattice. *New Journal of Physics*, 14(6):065002, 2012.

[18] F. Baboux, L. Ge, T. Jacqmin, M. Biondi, E. Galopin, A. Lemaître, L. Le Gratiet, I. Sagnes, S. Schmidt, H. E. Türeci, A. Amo, and J. Bloch. Bosonic condensation and disorder-induced localization in a flat band. *Phys. Rev. Lett.*, 116:066402, Feb 2016.

[19] Sebabrata Mukherjee, Alexander Spracklen, Debaditya Choudhury, Nathan Goldman, Patrik Öhberg, Erika Andersson, and Robert R. Thomson. Observation of a localized flat-band state in a photonic lieb lattice. *Phys. Rev. Lett.*, 114:245504, Jun 2015.

[20] Rodrigo A. Vicencio, Camilo Cantillano, Luis Morales-Inostroza, Bastián Real, Cristian Mejía-Cortés, Steffen Weimann, Alexander Szameit, and Mario I. Molina. Observation of localized states in lieb photonic lattices. *Phys. Rev. Lett.*, 114:245503, Jun 2015.

[21] Kazuto Noda, Akihisa Koga, Norio Kawakami, and Thomas Pruschke. Ferromagnetism of cold fermions loaded into a decorated square lattice. *Phys. Rev. A*, 80:063622, Dec 2009.

[22] N. Goldman, D. F. Urban, and D. Bercioux. Topological phases for fermionic cold atoms on the lieb lattice. *Phys. Rev. A*, 83:063601, Jun 2011.

[23] Shintaro Taie, Hideki Ozawa, Tomohiro Ichinose, Takuei Nishio, Shuta Nakajima, and Yoshiro Takahashi. Coherent driving and freezing of bosonic matter wave in an optical lieb lattice. *Science Advances*, 1(10), 2015.

[24] R. E. Peierls. On the theory of diamagnetism of conduction electrons. *Z. Phys 80 (World Scientific)*, 1933.

[25] Douglas R. Hofstadter. Energy levels and wave functions of bloch electrons in rational and irrational magnetic fields. *Phys. Rev. B*, 14:2239–2249, Sep 1976.

[26] Copyright 2015 The MathWorks, Inc. MATLAB and Simulink are registered trademarks of The MathWorks, Inc. See www.mathworks.com/trademarks for a list of additional trademarks. Other product or brand names may be trademarks or registered trademarks of their respective holders.

[27] H. R. Reiss. arxiv:1302.1212 [quant-ph], Jan 2013.

[28] M. V. Berry. Quantal phase factors accompanying adiabatic changes. *Proceedings of the Royal Society of London. Series A, Mathematical and Physical Sciences*, 392(1802):45–57, 1984.